Asia Pacific Research Initiative for Sustainable Energy Systems 2017 (APRISES17)

Office of Naval Research
Grant Award Number N00014-18-1-2127

Ocean Thermal Energy Conversion (OTEC) Heat Exchanger Development
(August 2021 - July 2022)

Task 5

Prepared for
Hawai‘i Natural Energy Institute

Prepared by
Makai Ocean Engineering

August 2022

HNEI
Hawai‘i Natural Energy Institute
University of Hawai‘i at Mānoa

MAKAI OCEAN ENGINEERING

ANNUAL REPORT

Prepared For

HAWAII NATURAL ENERGY INSTITUTE

1680 East West Road, POST 109

Honolulu, HI, 96822

USA

Prepared By

MAKAI OCEAN ENGINEERING

PO Box 1206, Kailua, Hawaii 96734

August 2022

TABLE OF CONTENTS

LIST OF FIGURES

LIST OF TABLES

1. INTRODUCTION

Makai Ocean Engineering has been developing Thin Foil Heat Exchangers (TFHX) for use in seawater-refrigerant, air-water, and water-water applications. This report summarizes work performed between August 2021 – June 2022.

In this period, Makai's efforts focused on improving TFHX fabrication success, developing TFHX production quality control methods, and continuing with thermal, hydraulic, and mechanical/structural characterization.

TFHX Design and Characterization. In this period, Makai introduced different materials and additional weld parameters and designs that expanded TFHX pressure capacity and channel sizes and began geometric and mechanical characterization of these new combinations. A welding analysis tool was also developed to guide optics and weld parameter selection. A new insert and sealing method, which is compatible for high operating temperatures and pressures, was also tested.

TFHX Fabrication. Makai focused fabrication efforts on improving success rates to achieve reliable, repeatable, high-quality TFHX plates. This required revisions to improve existing fabrication equipment and fixturing and new tooling and methods to monitor, evaluate, and repair TFHX plates during and after fabrication. Makai also commissioned the cutting station to remove the excess foil after a TFHX plate is fabricated.

All-Welded Design. Makai advanced the all-welded TFHX (AW-TFHX) technology by demonstrating the internal manifold weld. Makai completed the design and procurement of fixturing to weld and pressure test stacks of all-welded plates.

Stand-Alone TFHX Demonstration. In this period, Makai tested three ammonia-seawater (OTEC) TFHXs and three seawater-seawater (SWAC) TFHXs. Makai also started a long-term biofouling test.

2. TFHX DESIGN AND CHARACTERIZATION

In this period, Makai's TFHX design efforts included fabricating plates from a new material, a high temperature/high pressure compatible manifold insert design, new weld patterns and welding modes, a weld analysis tool to guide weld parameter selection, and improved equipment and software to characterize the internal channel size.

2.1. MATERIAL SELECTION AND WELD DESIGN

Makai has fabricated TFHX plates from titanium, stainless steel 316L, and, most recently, Haynes 230. Makai developed a Weld Thermal Analysis program to aid in weld parameter selection based on the material properties and weld pattern design.

2.1.1. Material Selection

Makai has demonstrated the TFHX can be fabricated using titanium, stainless steel (316L), and nickel-based alloys (Haynes 230). Each material has different thermal, mechanical, and chemical properties, as well as different cost. Makai's ability to construct TFHXs from a range of materials expands opportunities for the TFHX.

For example, Makai demonstrated TFHX fabrication was compatible with Haynes 230, a nickel-based alloy used in high temperature, high pressure applications. Haynes 230 is an expensive material and a conventional Haynes 230 heat exchanger is not cost effective. However, because the TFHX design enables significantly less material usage compared to conventional heat exchangers, Haynes 230 TFHX may deliver the same temperature and strength performance and provide cost savings.

2.1.2. Weld Thermal Analysis Program

Initial TFHX development work was conducted on 0.003" and 0.004"-thick titanium foil. When Makai started using 0.005"-thick titanium foil and different materials (SS316L or Haynes 230) at the same foil thicknesses (0.003" or 0.004"), it was apparent that new weld parameters were necessary. Methodical testing of weld parameter combinations became impractical; the further the material and foil-thickness combination was from the initial 0.003" titanium foil, the more combinations had to be tested.

Makai developed a Weld Thermal Analysis Program to simulate whether a set of weld parameters is likely to produce a high quality weld.

A good weld is defined by the following characteristics:

- Full penetration depth: the melt pool extends fully through both pieces of foil to produce a weld that is two foil-thicknesses deep
- No material loss: the foil surface temperature is maintained below the material boiling point so little or no material is lost through vaporization.

The Weld Thermal Analysis Program uses a finite-element model and transient heat transfer properties to balance the laser energy input at each time step to calculate foil temperature profile.

2.1.3. Welding Modes

In addition to determining the right combination of weld parameters, there are also options to select the type of weld being performed. In this period, Makai tested out a new wobble mode which rotates a spot weld around a point to create a larger dot weld or a circle weld by specifying a radius, frequency of rotation, and laser firing time.

2.1.4. Hexagonal Pattern

One major advantage of the TFHX over conventional heat exchangers is the ability to customize both fluid channels to optimize performance. The pattern weld portion of a TFHX plate is used for the main heat transfer area. The pattern weld sets the internal fluid channel size and, therefore, the thermal and hydraulic performance of the TFHX. In this period, Makai introduced a hexagonal pattern weld which enables a larger internal channel. For the same plate spacing, a plate with a hexagonal weld pattern could be stacked with a triangular weld pattern plate and to create smaller external channels than stacking two triangular weld pattern plates.

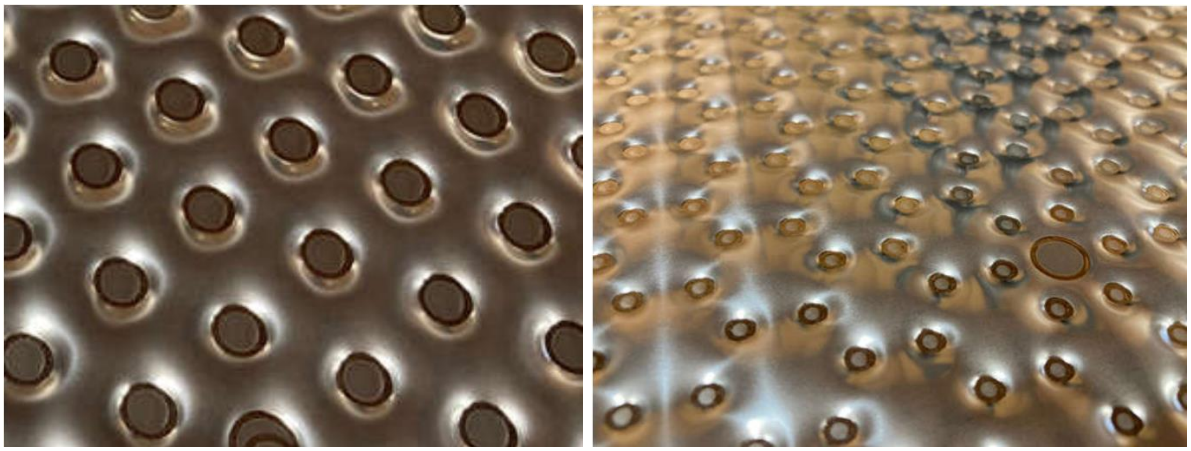

Figure 1. Triangular pattern (left) and hexagonal pattern (right). The hexagonal pattern enables larger internal channels.

2.2. HIGH TEMPERATURE SEALING

Makai designed a new sealing method suitable for high-temperature, high-pressure applications. The existing method is limited to < 121°C; for higher temperature applications, Makai is pursuing the use of metal seals.

Makai performed a preliminary test by pressuring a small stack of test plates to over 2000 psig. Leaks were identified, although the precise leak location was obscured. Upon disassembly and inspection, Makai suspects the leaks were due to inadequate contact between the sealing surfaces (Figure 2).

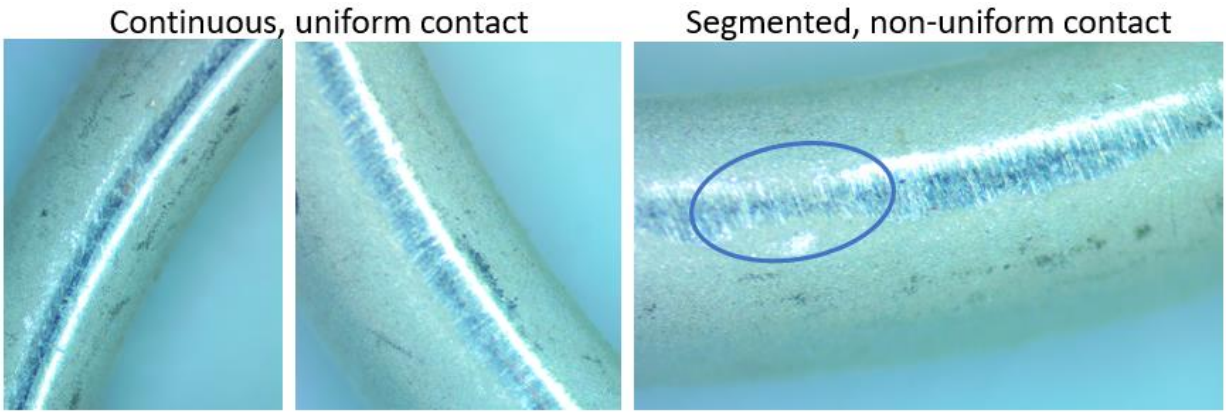

Figure 2. Non-uniform contact along c-ring surface.

2.3. MECHANICAL CHARACTERIZATION

A key advantage of the TFHX is that each individual plate meets the pressure rating without external support. In addition to being able to meet a specified pressure rating, a TFHX unit is subject to cyclic pressures during operation and must meet a minimum lifetime. Supported and unsupported burst pressures are used to establish the pressure rating and predicted lifetime of a heat exchanger. Fatigue life is a function of both design and loading conditions.

2.3.1. Static Pressure Testing

Burst pressure testing includes supported and unsupported tests. In a supported burst pressure test, a welded plate is placed in the expansion fixture where it is clamped on all sides with the hydraulic press. The plate is expanded until failure and the pressure at failure is recorded as the supported burst pressure. In the unsupported test, a finished plate (welded, formed, and excess foil removed) is put into a fixture in which only the manifolds are clamped (to provide the seal for pressurization with compressed air or water) and expanded until failure.

In general, tighter weld spacings, larger weld diameters, and thicker foils produce higher supported burst pressures (Figure 3). In many tests, the burst location was at a transition weld or unidentified location; these points are plotted using different symbols to distinguish from pattern weld burst locations. In most situations, transition welds can be modified and strengthened such that the true limitation of the pattern weld design is tested.

As observed in supported burst pressures, tighter weld spacings, larger weld diameters, and thicker foils lead to higher supported burst pressures (Figure 4). For the titanium foil thicknesses tested, unsupported burst pressure increased linearly with foil thickness (Figure 5).

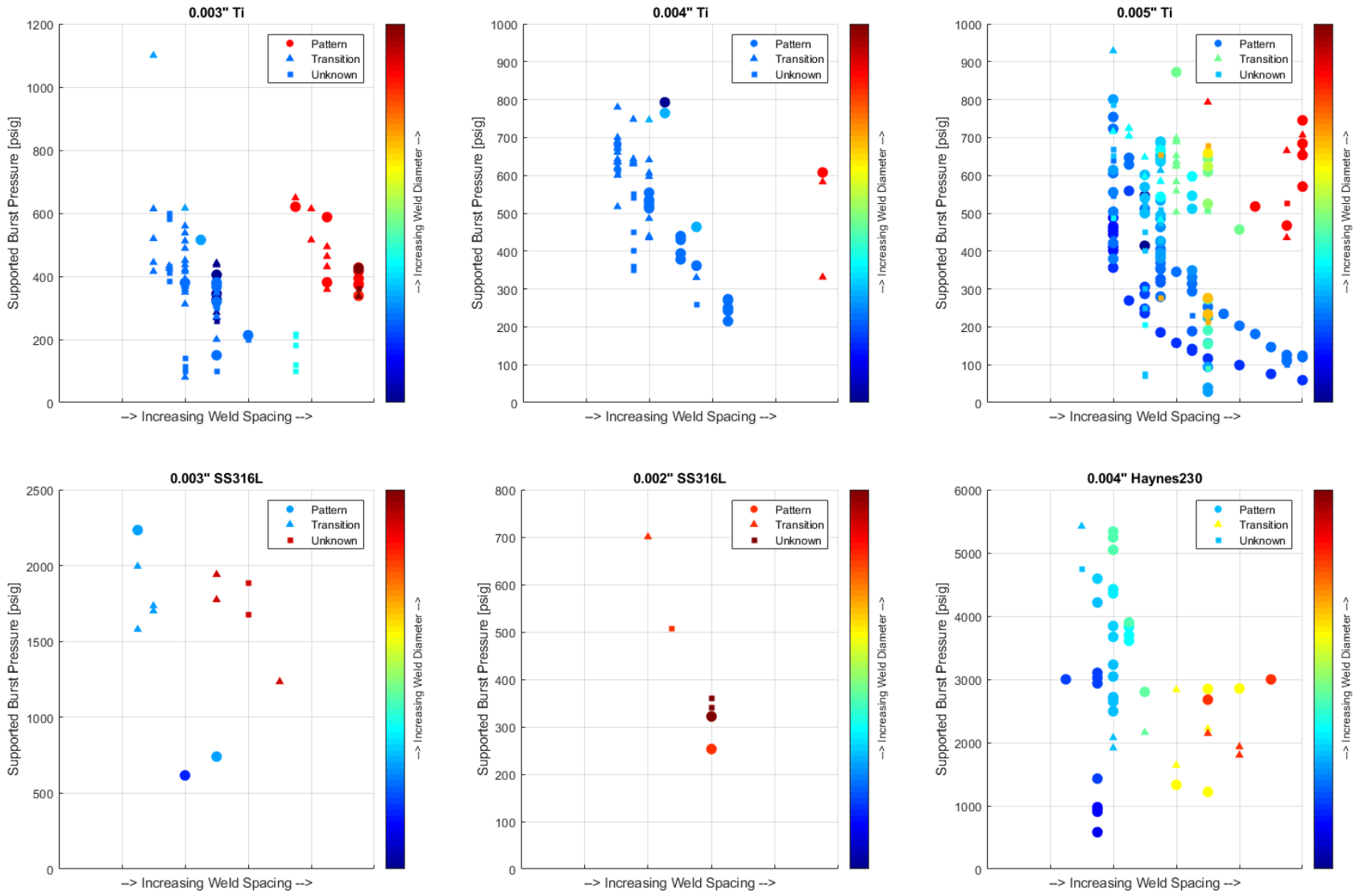

Figure 3. Supported burst pressure dependence on weld spacing, weld diameter, material, and foil thickness.

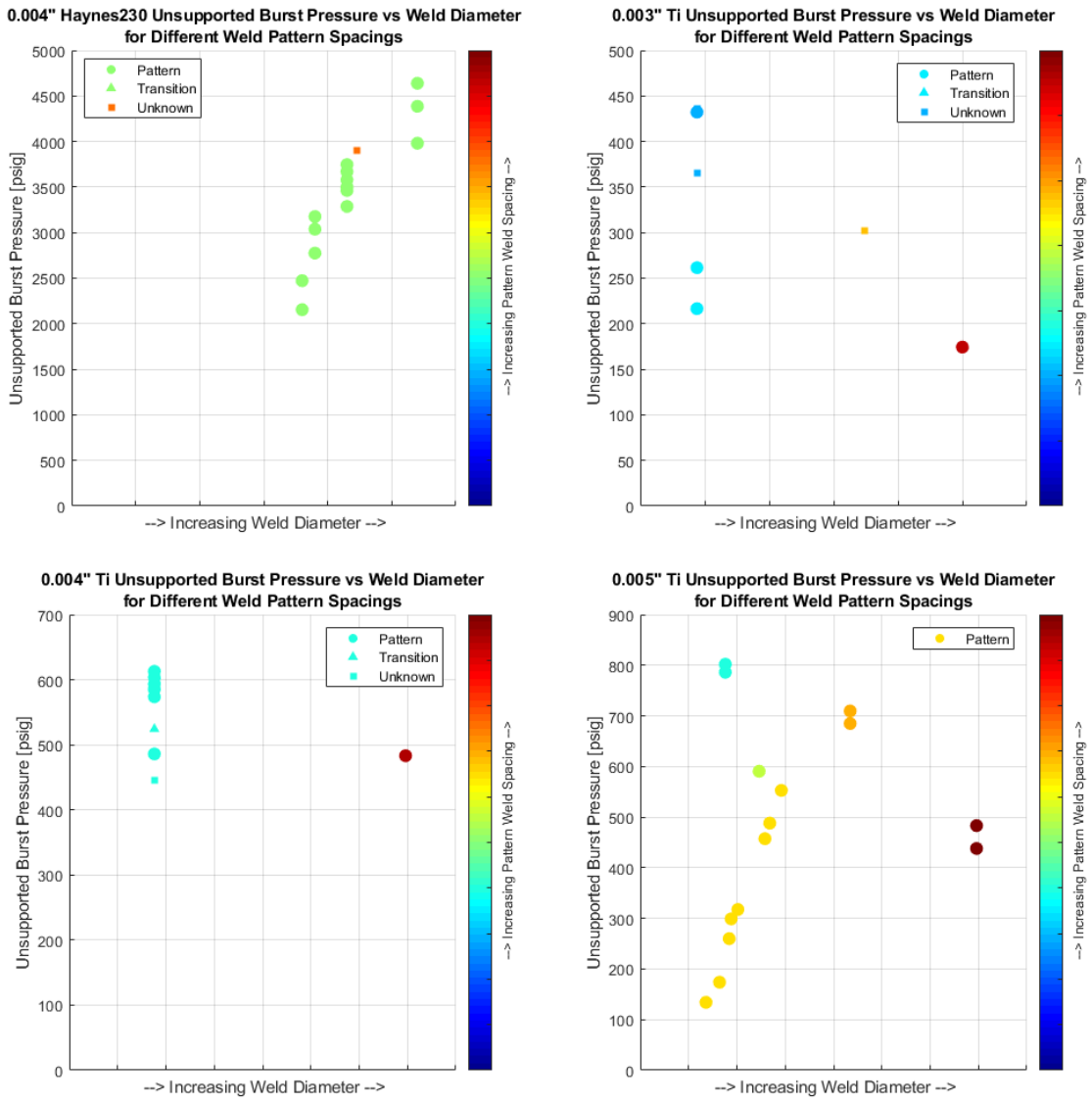

Figure 4. Unsupported burst pressures for varying foil thicknesses, weld diameters, and weld spacings.

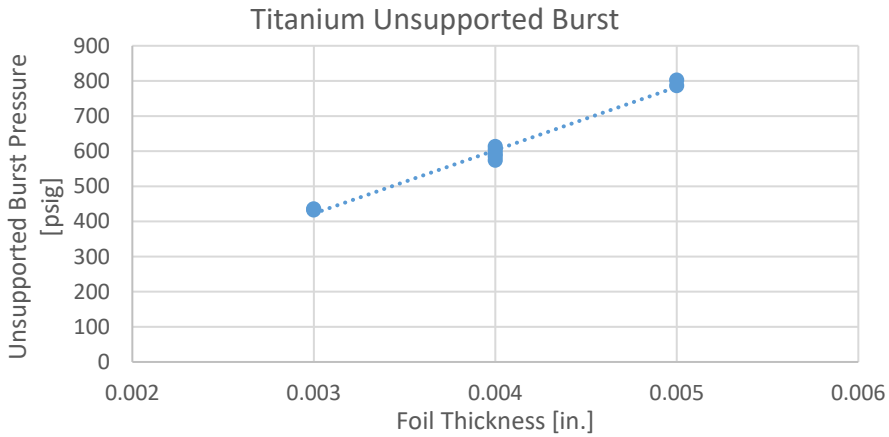

Figure 5. Unsupported burst pressure of 0.003", 0.004", and 0.005" with the same weld pattern design.

2.3.2. Cyclic Pressure Testing

Previously reported fatigue testing results suggested fatigue life is extended by reducing the alternating pressure, reducing the pattern spacing, and increasing the foil thickness. Makai also tried to establish a relationship between fatigue life and alternating pressure as a function of unsupported burst pressure but suspected preliminary results (Figure 6) may be biased by fixturing design and non-optimal weld parameters.

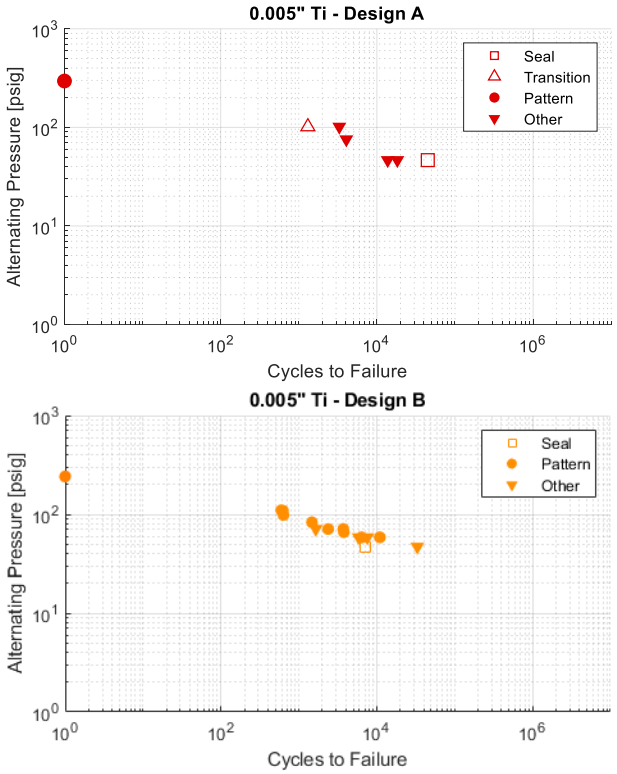

Figure 6. Fatigue life of two different 0.005" Ti plate designs.

Makai established a test plan to determine:

- For the same weld pattern spacing, is fatigue life affected by weld diameter?
- For the same weld diameter, how does weld pattern spacing affect fatigue life?
- Are there other process steps that can improve fatigue life?

Four sets of weld designs will be used for the initial tests (Table 1). For each set of weld designs, four different process steps will also be tested to determine the effect on fatigue life.

Table 1. Fatigue Test Plan – Weld Designs

Design	Supported Burst Pressure [psig]	Un-supported Burst Pressure [psig]	Effective Height [mm]
1	520	436	0.652
2	590	515	0.619
3	524	415	0.632
4	367	289	0.845

Fatigue testing will be conducted from 60-160 psig, similar to previous testing for OTEC cycle pressures. For each design, three plates of each of the baseline process and four different process steps will be tested in fatigue (16 plates for each design). Makai has started testing on the first weld design set and found a fatigue life increased with the process steps, lasting up to three times longer than the other samples (Figure 7). For this set of weld design parameters, all failures have occurred in the pattern weld, indicating limitations of the pattern weld rather than the manifold, seal, or transition weld, are tested.

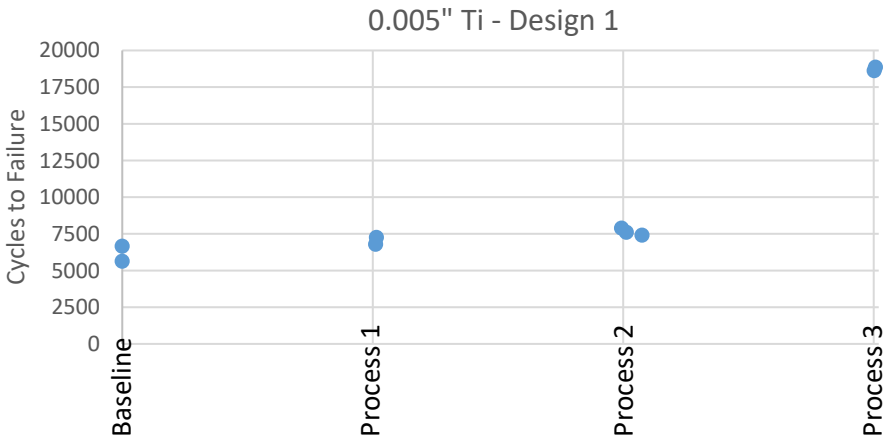

Figure 7. Fatigue life for baseline and three different process steps for 0.005" Ti plate.

Once all four weld designs and process steps have been tested, the next steps are to use the best design to determine whether fatigue life can be predicted as a function of the alternating pressure to unsupported burst pressure ratio.

2.4. GEOMETRIC CHARACTERIZATION

With geometric characterization, the goal is to establish the design parameters – material, foil thickness, weld diameter, weld spacing, and expansion pressure – required to create a specific internal channel size and shape. In this period, Makai continued characterization studies for titanium and began studies for stainless steel and Haynes 230. The same trends were observed, namely, larger weld spacings, thinner foils, higher expansion pressures, and smaller weld diameters produced larger effective internal channel heights.

Makai improved the process of measuring the plate by upgrading from a single point measurement profilometer to a 2D scanner, which records the heights under a 20-mm line. The new scanner is integrated into the HSWS and can also take measurements at different stages during expansion. A custom Labview program was developed to analyze the scanner data and calculate the effective internal channel height. With the larger scan window, a background plane can also be subtracted from the measurement section to provide a more accurate effective channel height calculation.

Using data from the 2D scanner, a secondary program was developed to visualize the external channel when two plates are stacked together (Figure 8). This program aids in evaluating whether the plates will interfere (i.e., the peak channel height is too large for the plate spacing) and also calculates the effective external channel size.

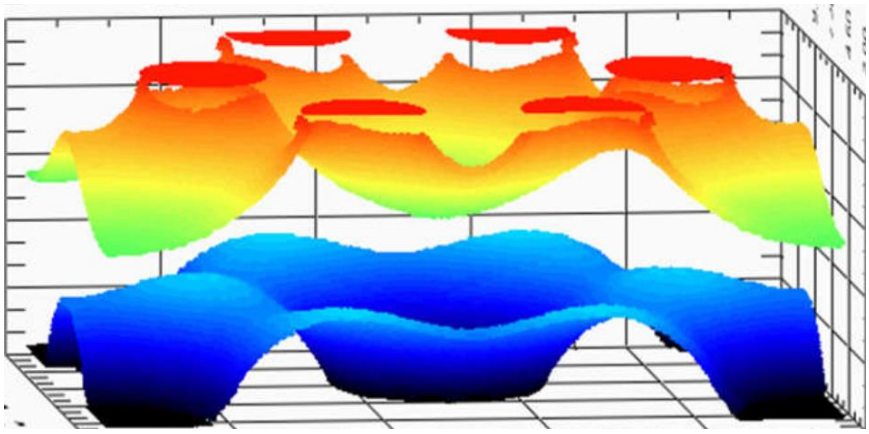

Figure 8. Visualization of two plates stacked together using data from 2D scanner.

In general, thinner foils, smaller welds, larger weld spacings, and higher expansion pressures produce larger effective channels. For example, in Figure 9, for 0.004” Ti, lower expansion pressure is required to produce a 0.2mm effective channel for smaller weld spacings (light blue points) compared to larger weld spacings (dark blue points) for the same weld diameter (small dots).

Performance requirements, typically pressure drop, drive the effective internal channel size specification but pressure rating and fatigue life must also be considered choosing the combination of foil thickness, weld diameter, weld spacing, and expansion pressure.

For 0.003”-0.005”-thick titanium foils, Makai has been able to use previously collected data to reasonably estimate the required weld spacing and weld diameter to produce a specified effective channel spacing. However, new materials and foil thicknesses still require characterization.

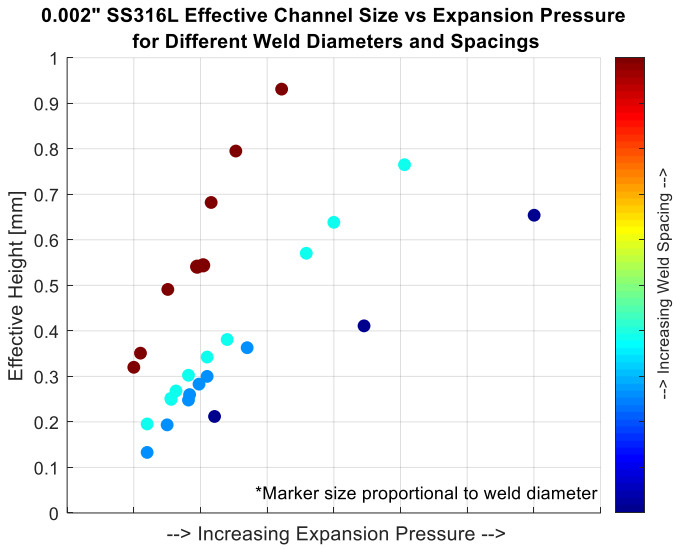
0.002" SS316L Effective Channel Size vs Expansion Pressure
for Different Weld Diameters and Spacings
Effective Height [mm]
--> Increasing Expansion Pressure -->
--> Increasing Weld Spacing -->
*Marker size proportional to weld diameter

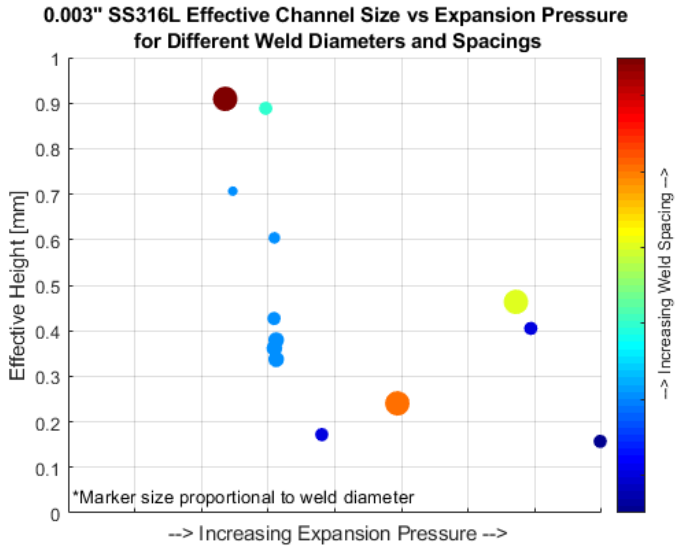
0.003" SS316L Effective Channel Size vs Expansion Pressure
for Different Weld Diameters and Spacings
Effective Height [mm]
--> Increasing Expansion Pressure -->
--> Increasing Weld Spacing -->
*Marker size proportional to weld diameter

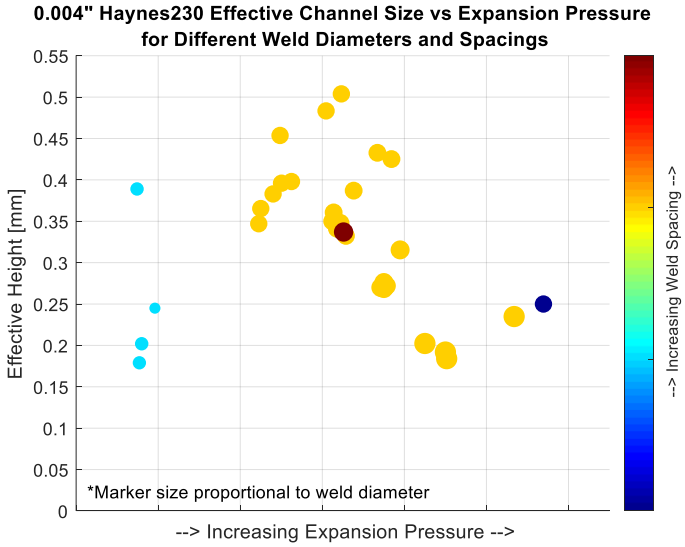
0.004" Haynes230 Effective Channel Size vs Expansion Pressure
for Different Weld Diameters and Spacings
Effective Height [mm]
--> Increasing Expansion Pressure -->
--> Increasing Weld Spacing -->
*Marker size proportional to weld diameter

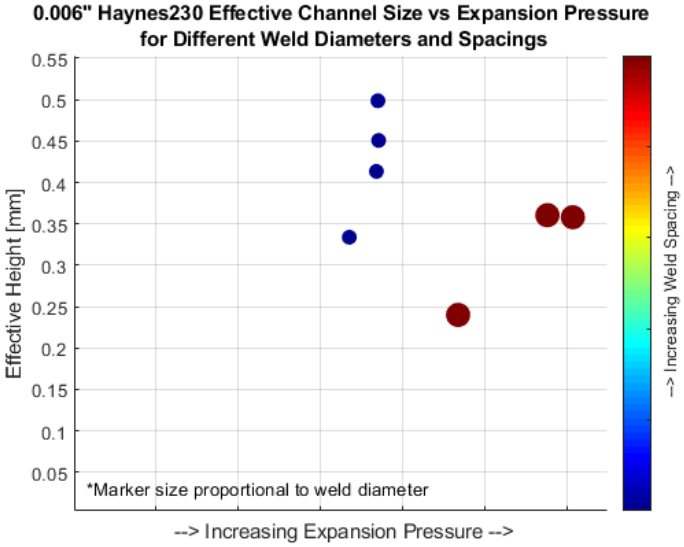
0.006" Haynes230 Effective Channel Size vs Expansion Pressure
for Different Weld Diameters and Spacings
Effective Height [mm]
--> Increasing Expansion Pressure -->
--> Increasing Weld Spacing -->
*Marker size proportional to weld diameter

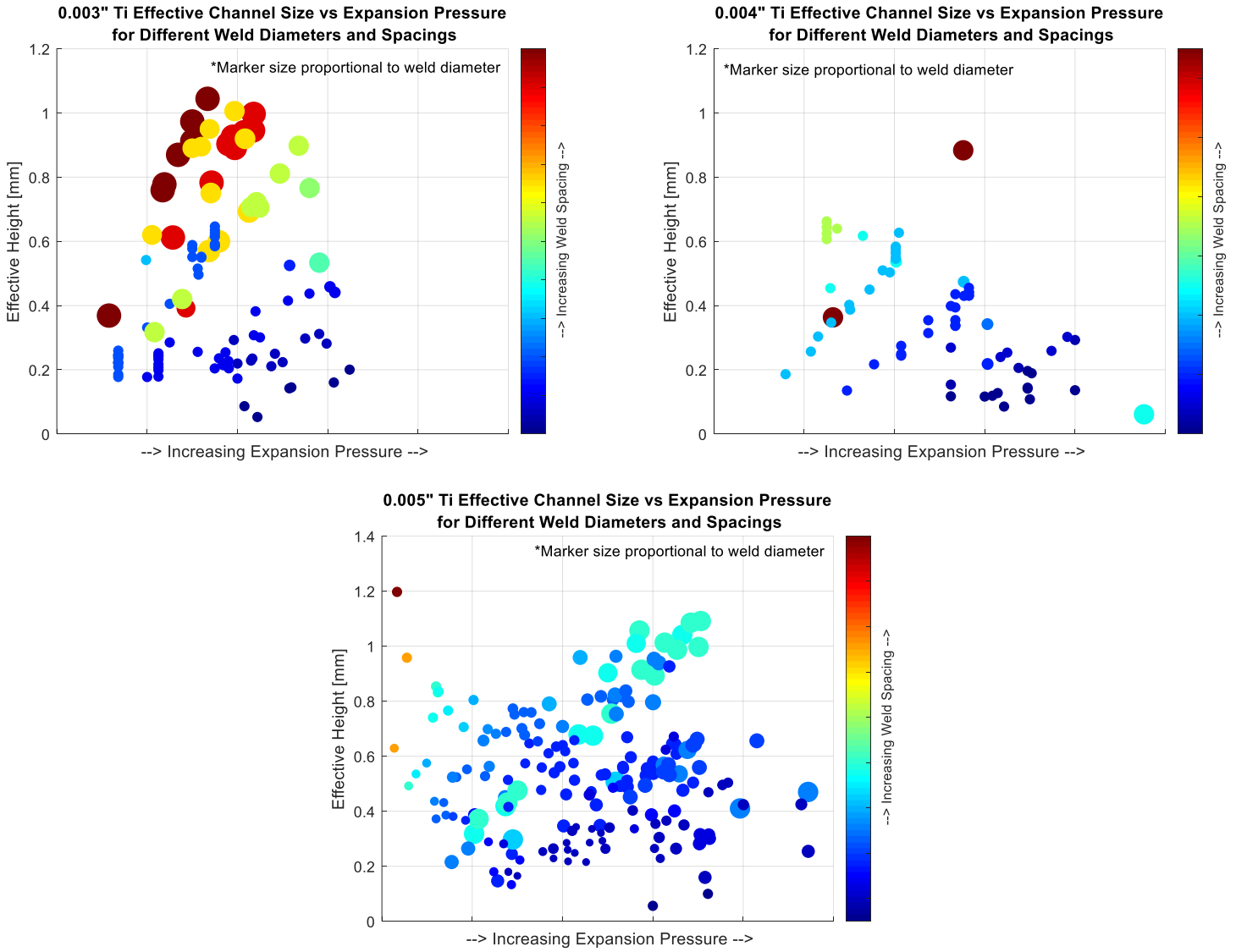

Figure 9. Effective internal channel height for different materials, foil thicknesses, and design parameters. Marker size is proportional to weld diameter; larger markers indicate larger welds.

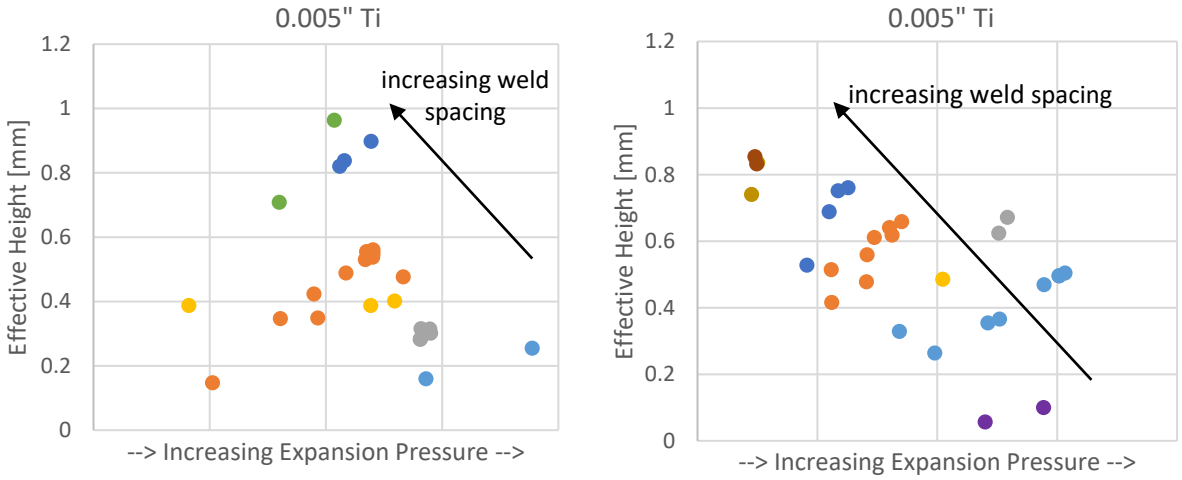

Figure 10. For the same weld diameter, larger weld spacings and higher expansion pressures produce larger effective channels.

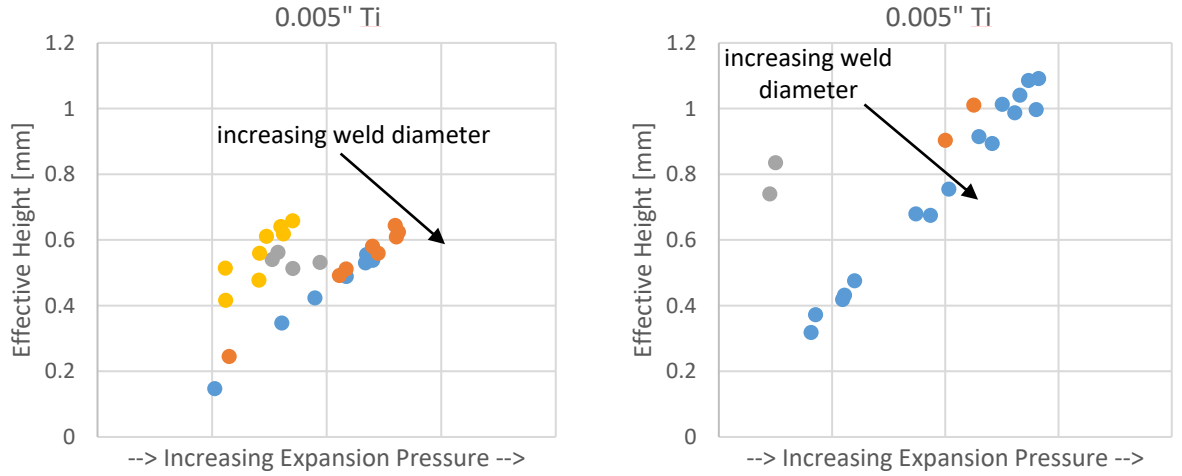

Figure 11. For the same weld spacing and expansion pressure, larger weld diameters produce smaller effective heights.

3. TFHX FABRICATION

Makai focused fabrication efforts on improving success rates to achieve reliable, repeatable, high-quality TFHX plates. This required revisions to improve existing fabrication equipment and fixturing and new tooling and methods to monitor, evaluate, and repair TFHX plates during and after fabrication. Makai also commissioned the cutting station to remove the excess foil after a TFHX plate is fabricated.

3.1. FABRICATION PROCESS IMPROVEMENTS

Shortly after commissioning the High Speed Welding Station (HSWS), Makai began to fabricate full-length (1-m long) titanium TFHX plates with ~50% success rate, which was a significant departure from the over 99.99% success rate when fabricating on the stage.

Makai is attempting to improve the fabrication success rate by incorporating design improvements to the fabrication fixturing, developing methods monitor weld quality, and developing techniques to repair welds.

3.2. WELD QUALITY CONTROL

Repairing defective welds is another way to produce a successful plate and improve the overall success rate. The first step in quality control is to establish methods to identify defective welds.

3.2.1. High Speed Pressure Tester (HSPT)

Most of the failed plates had only one weld defect and the defect could not always be identified by visual inspection under a microscope. A soap bubble check is usually the fastest way to find a leak; Makai designed a High Speed Pressure Tester (HSPT), in which a plate can be installed and pressurized in 10 seconds, to quickly identify leaks. The frame of the HSPT is open so the top and backside is accessible for leak detection/identification. For leak checks, the plate is held at pressure for at least 30 seconds or as long as necessary to identify leak locations. A microscope fitted with a digital camera is mounted at the HSPT to document failures.

The HSPT will also be used as the unsupported burst pressure tester and fatigue tester for full-length plates. To more accurately mimic the plate condition in a heat exchanger, a backing and top plate were designed to simulate the effect of adjacent plates in a heat exchanger, which restrict the degree a single plate can deform in the unsupported condition.

3.2.2. Imaging

A major component of Makai's weld quality program will rely on machine vision/machine learning to identify weld defects through high-resolution images of welds. Ideally, weld images are taken and processed by the completion of the welding step and potentially weak welds are repaired prior to the next step in fabrication. High resolution imaging of 10,000+ welds in real-time in the HSWS is not a straightforward task. Camera and lighting options must be selected so the different weld locations, weld types, and weld defects can be reliably imaged.

Makai has performed preliminary testing and was able to identify weld defects under different conditions. Makai is still testing different weld types and different failure types to determine the best set of conditions for imaging.

3.3. WELD REPAIR

Repair entails sealing off the defect with a larger weld. A weld repair prior to forming the internal channels is preferred because the plate is still in the same position and the defective weld location is indexed to the same reference. Repair after forming the internal channels requires an extra step; the defective area must be crimped, patched and then welded to seal the defect.

Presently, weld repair requires manual identification of weld defects, by visual inspection or using a leak check in the HSPT. Makai's is working on an algorithm to automatically identify and eventually repair welds without operator input.

3.4. CUTTING STATION

Makai verified that laser cutting was a viable method to remove the excess foil around the seal weld of completed TFHX plates. Makai then commissioned a dedicated, stand-alone cutting station in the new fabrication facility.

The cutting station has a 1.2m x 1.2m working area. An optical table provides the mounting reference and Zaber stages (two Y-stage gantries, an X-stage, and a Z-stage) are used to move the cut head to programmed locations. Custom Labview software was developed to control the stage, laser, and laser support systems so the entire cutting process is automated. The operator only needs to install/remove the TFHX plate and initiate the cut program, the remaining steps are automated. A full-length TFHX plate requires 90 seconds to cut; 20 seconds is installing/removing the plate and the remaining 70 seconds is cutting process.

Two issues were identified during commissioning and use of the cutting station. First, the mounting brackets for the cut head weren't stiff enough during acceleration (as required for circular cuts), resulting in oscillations and wavy cut paths (Figure 12). Second, on longer straight cuts, the cut edge was observed to have a slight slant instead of being parallel with the seal weld. Upon investigation, the linear Y-stage has a slight bow towards the end of travel, which forces the slanted cut path when a straight path is specified. The cut head mount has been re-designed and a new linear stage was ordered.

Figure 12. The cut head mount wasn't stiff enough to prevent oscillations during accelerations required for circle cuts, resulting in a wavy cut.

Prior to commissioning the dedicated cutting station, plates cut on the stage frequently had beading and/or burrs along the cut edge (Figure 13). These burrs required manual removal with a deburring tool because the rough edges increase the external pressure drop and also can interfere with fit inside the housings. Since the dedicated cutting station was commissioned, the cut edges have been mostly smooth and not required post-cut deburring (Figure 14).

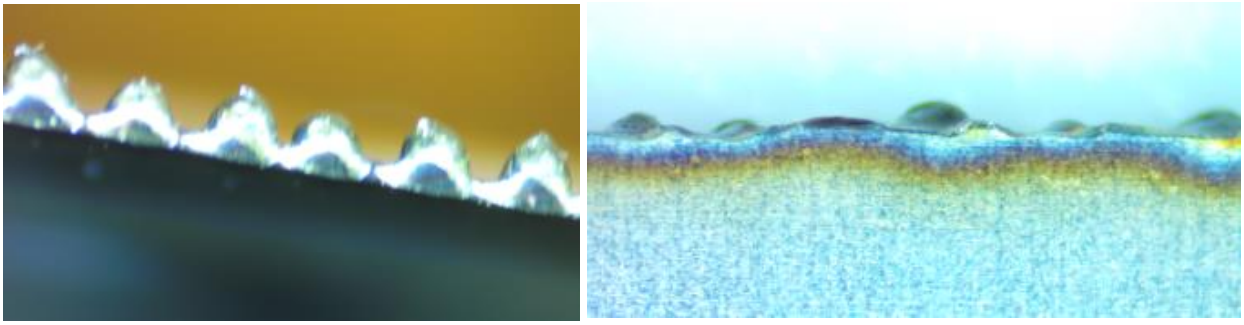

Figure 13. Burrs on the cut edge.

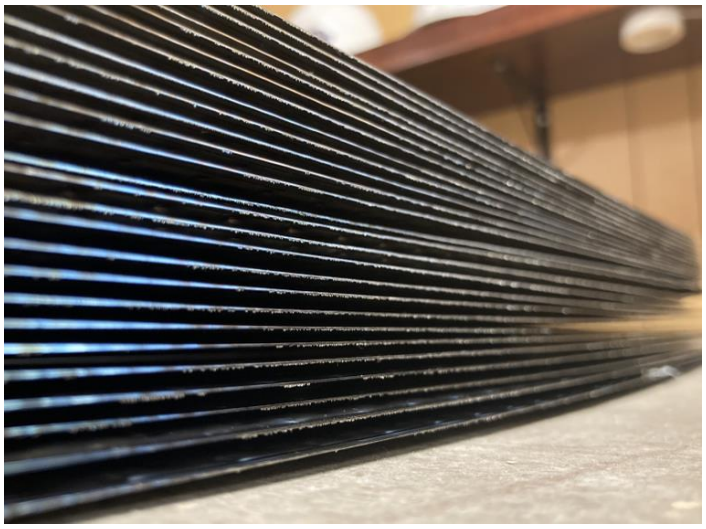

Figure 14. Cut edges on the commissioned cutting station are relatively smooth and do not require a post-cut manual deburring step.

4. ALL-WELDED DEVELOPMENT

Makai's goal for the All-Welded (AW) development in this period was to construct a sealed stack of 5 AW-TFHX plates. New fixturing, plate components, imaging equipment, and software were developed/procured to perform this work.

An AW-TFHX requires welding together the manifold openings of adjacent plates and welding the first and last plates to header/follower plates which supported interface connections for the internal fluid. Because the manifold welds for each plate is performed sequentially, Makai designed a stacking fixture to hold the stack of plates together and move the welded stack so that the focal plane for subsequent welds remained the same. The welding and stacking fixture were assembled and a calibration was performed to control the vertical position of the stage.

Different weld parameter combinations were tested to identify suitable combinations; because a seal test or burst test could not be performed, results were based on visual inspection of the weld (Figure 15).

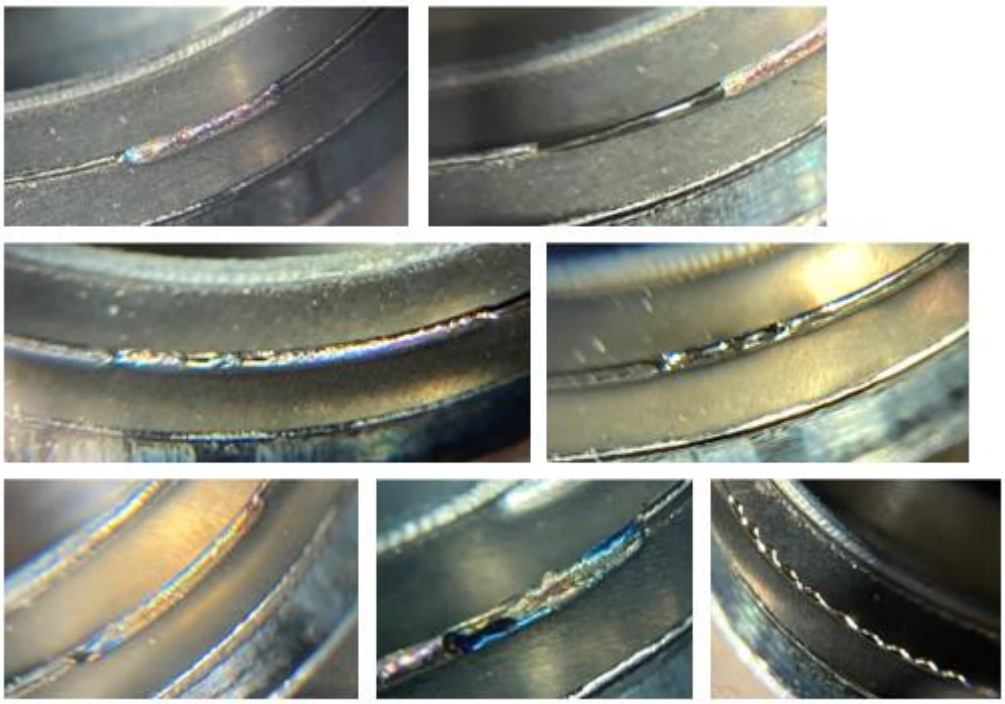

Figure 15. Visual inspection of welds performed using different parameters and shield gas flow rates reveals significant differences in weld quality. Smooth silver welds are preferred.

Makai attempted to fabricate a 5-plate AW-TFHX but was unable to demonstrate sealing. Based on the initial results, Makai concluded substantial effort is still required for an automated, reliable, and cost-effective laser-welded AW-TFHX. Makai has decided to explore alternate methods of achieving an AW-TFHX.

5. TFHX PERFORMANCE TESTING

In this period, Makai built 3 stand-alone TFHX units with different internal/external channels and plate spacings (Table 2). Each unit was tested in a counterflow configuration as a condenser, an evaporator, and a seawater-seawater (SWAC) heat exchanger (Figure 16). Makai also started a baseline biofouling test using FL1.

Table 2. Overview of TFHX test units.

Unit	# Plates	Plate Spacing [mm]	Foil Thickness ["]	Internal Channel [mm]	External Channel [mm]	Fluid Length [m]	HX Area [m^2]
FL1	24	2.12	0.005	0.59	1.28	0.86	10.32
FL2	24	2.12	0.005	0.9	0.97	0.86	10.32
FL3	12	4.24	0.005	0.9	3.08	0.86	5.16

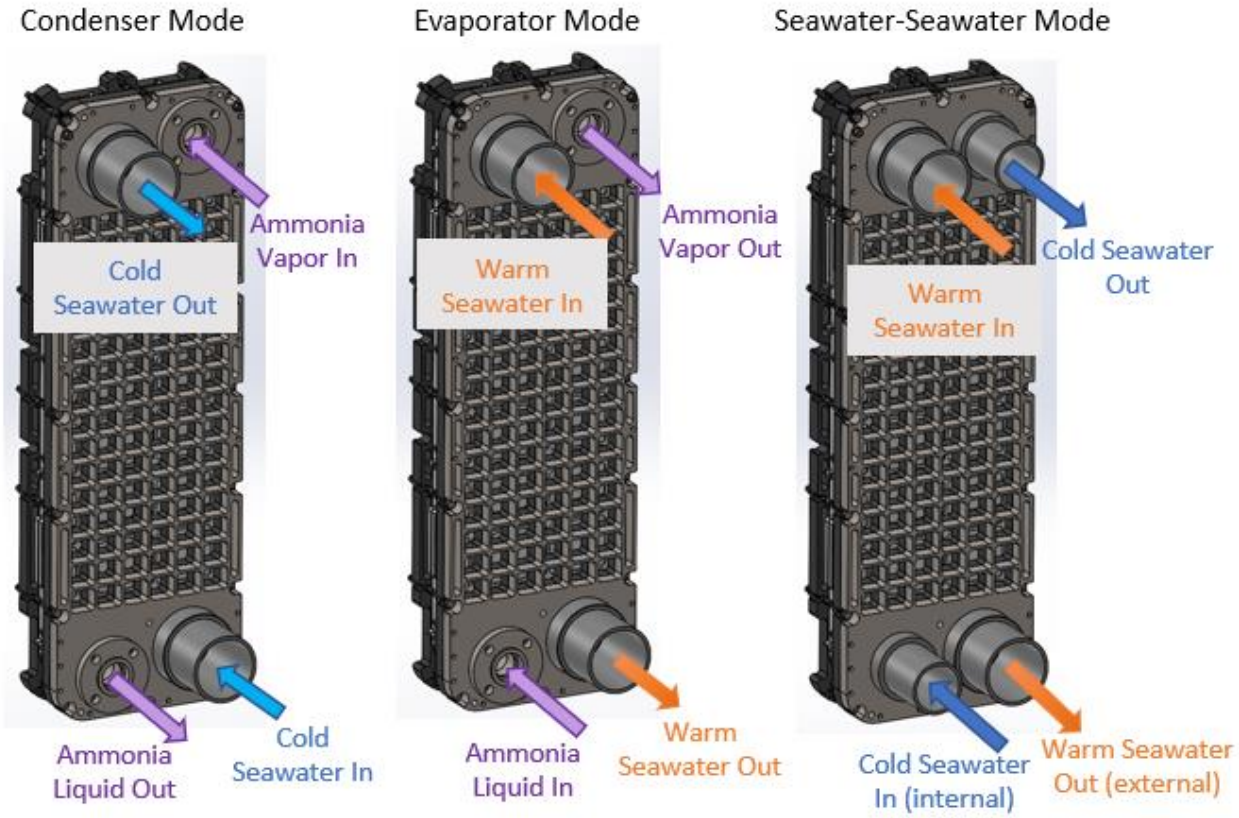

Figure 16. Full-length TFHX module configured for counterflow condenser, evaporator, and seawater-seawater (SWAC) testing.

In order to test at twice the plate spacing, FL3 used spacers shown in Figure 17 for condenser and evaporator testing. The spacers provided an inlet/outlet manifold for ammonia and distributed

seawater flow evenly to the external channels. However, some discrepancies were observed in seawater pressure drop between condener and evaporator modes and upon diassembly, in some spacers, the spacers were rotated out of position and the side with the seawater (external) manifold openings was torn (Figure 17). The spacers and TFHX plates were modified prior to seawater-seawater testing to only use spacers for the internal fluid manifold (Figure 18).

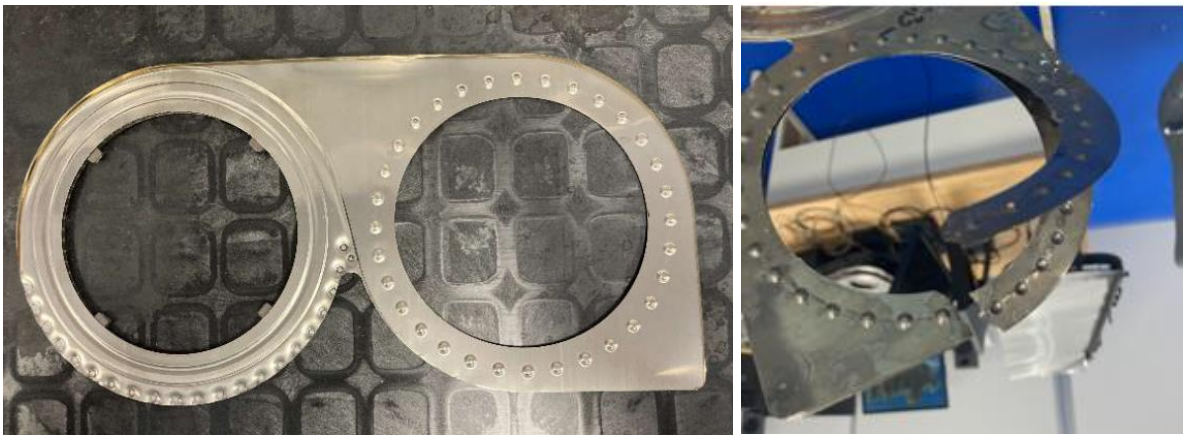

Figure 17. (left) FL3 spacers for condenser and evaporator testing. (right) The external fluid opening of several spacers was found to have rotated out of position and a few were also torn after testing.

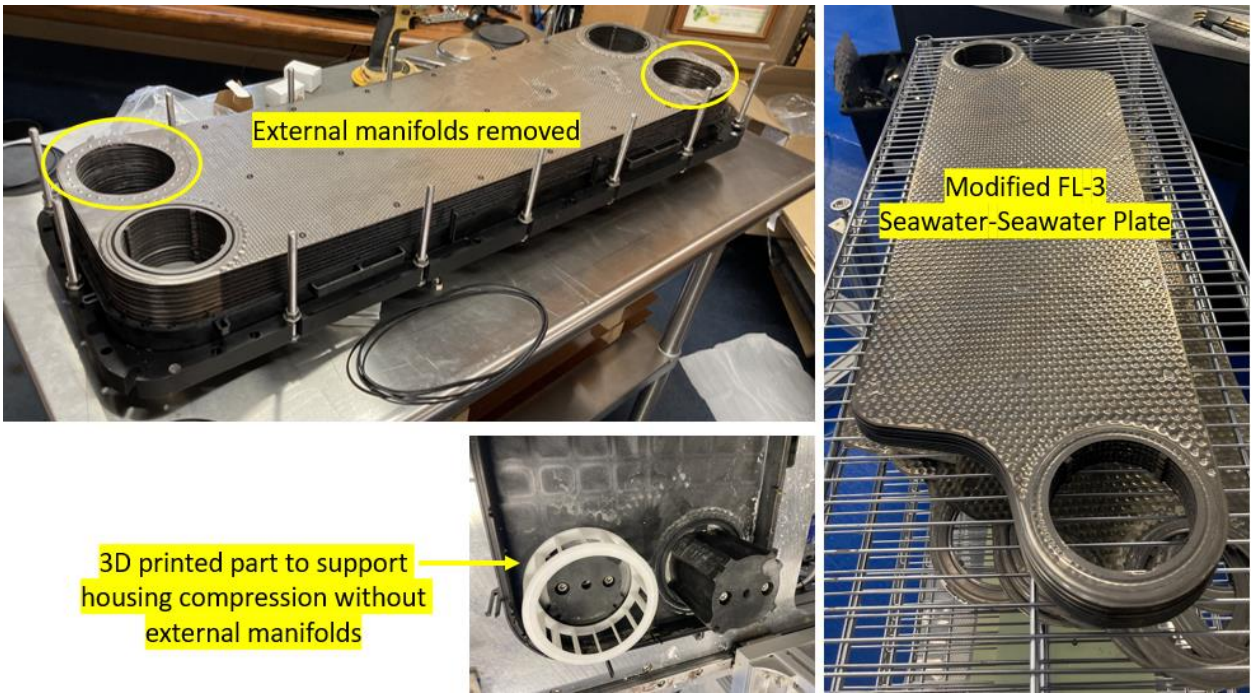

Figure 18.Modifications to remove external manifolds in FL3 SWAC plates. Circular spacers were required for internal manifolds but were less likely to rotate out of position.

5.1. SEAWATER-AMMONIA AND SWAC TESTING RESULTS

In condenser and evaporator configurations, each heat exchanger was tested at energy densities between 5-20 kW/m^2 and seawater velocities between 0.3-1.3 m/s. Ammonia duty was controlled by controlling the seawater flow rate through the companion (APV) heat exchanger. For example, during evaporator testing, the APV heat exchanger functions as a condenser; increasing the cold seawater flow through the APV increases TFHX duty at a fixed TFHX seawater flow rate. Seawater flow was controlled by adjusting seawater control valves. During evaporator testing, the quality is set by adjusting the ammonia liquid flow rate using a VFD to control the feed pump.

In the SWAC configuration each heat exchanger was tested at 8-15 internal (cold) seawater velocities between 0.1-0.8 m/s and 10-20 external (warm) seawater velocities between 0.1-1.5 m/s. Some flow variation was observed due to changes in seawater supply pressure.

Detailed test points for each heat exchanger are tabulated in Appendix A.

5.1.1. Seawater Pressure Drop

Seawater-side pressure drop is related to the pumping power required to provide a certain seawater flow rate through the heat exchanger.

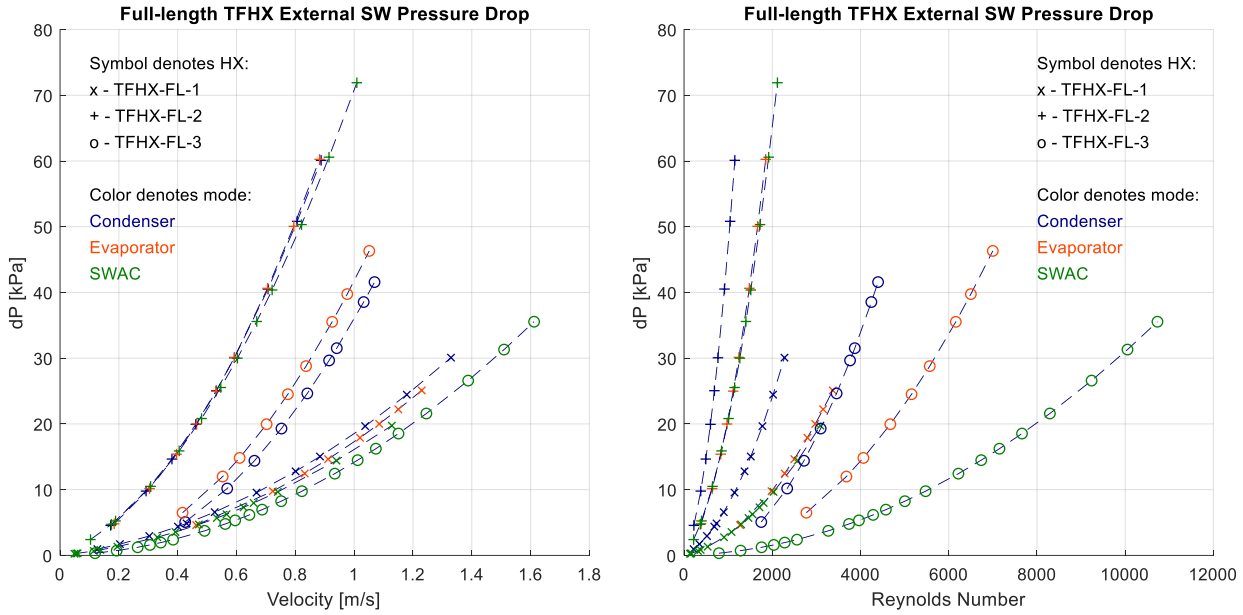

Figure 19. Seawater pressure drop for all three TFHX units. The FL3 SWAC data set is taken after the torn external spacers were removed.

Seawater pressure drop observed during FL3 evaporator and condenser testing (Figure 19) was abnormally high. The seawater channels in FL3 were larger than FL1, therefore at the same Reynolds number, the pressure drop is expected to be lower. The higher-than-expected pressure drop was attributed to the spacers rotating out of position. In FL3-SWAC, the external spacers were removed and the pressure drop decreased by over 2X. Makai also evaluated the contribution of entrance/exit losses, where the flow must turn perpendicularly to enter/exit the module, to the

overall pressure drop. The losses attributed to the components were calculated using minor loss coefficients reported in Table 3 and determined to have a small contribution to overall pressure drop in FL1 and FL2, but up to 25% of the pressure drop in FL3 due to the high volumetric flow rates associated with the larger channels in FL3.

Table 3. Minor loss coefficients

Component	Minor Loss Coefficient
90° turn	1.1
Pipe exit, sharp edged	1
Sudden contraction (into channels)	0.5
Sudden expansion (exit channels)	1
Pipe inlet, sharp edged	0.5
90° turn	1.1
Total	5.2

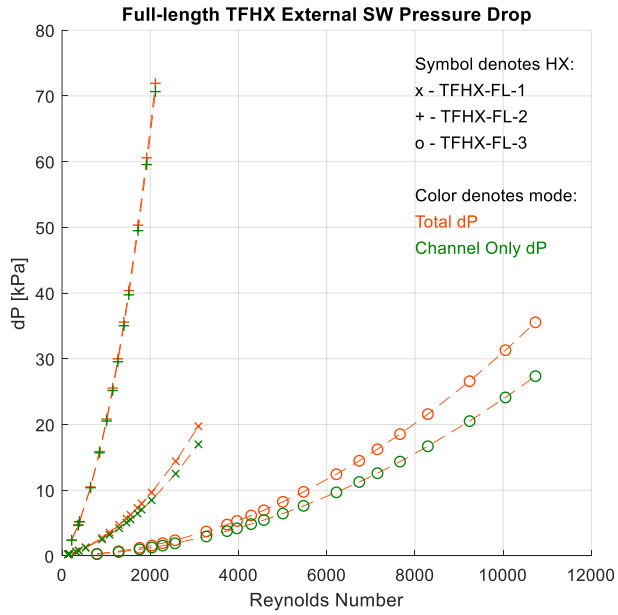

Figure 20. Contribution of minor loss components versus channel losses.

The internal seawater pressure drop is also important for SWAC operations. FL2 and FL3 had the same internal channel sizes and the internal pressure drops agree (Figure 21).

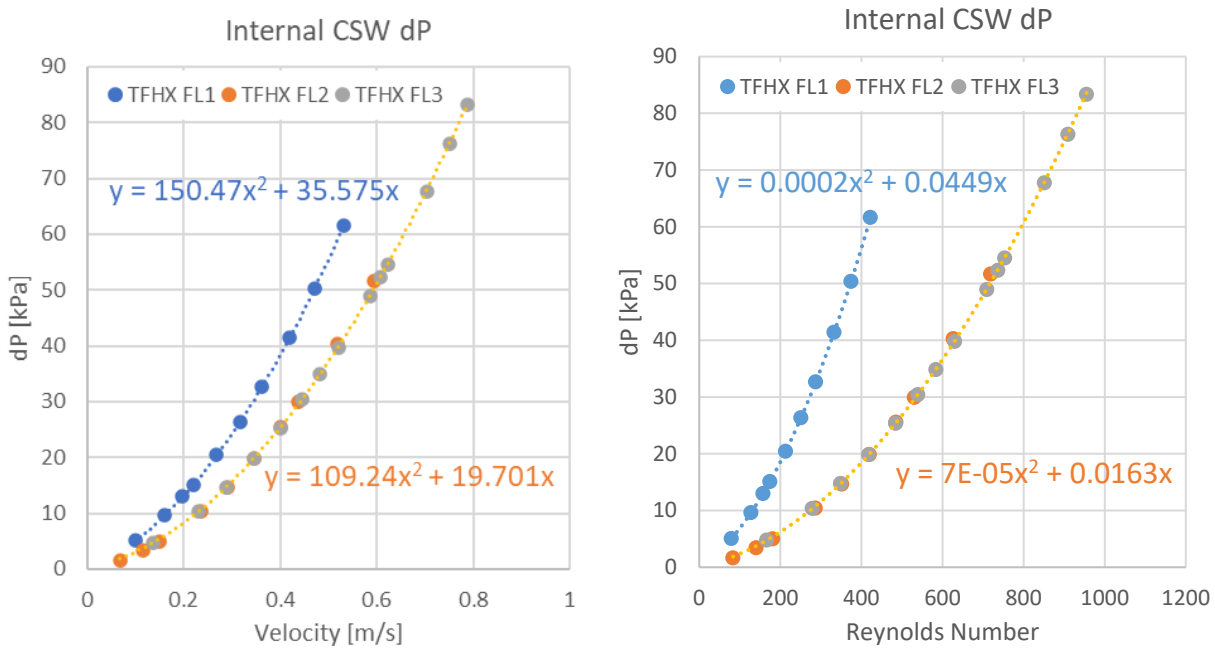

Figure 21. Internal seawater pressure drop for three TFHX designs.

Internal and external seawater pressure drops can be normalized by path length and compared to previous TFHX condensers, evaporators, and SWAC heat exchangers. The current FL1-FL3 TFHXs are 4-port designs compared to previous TFHX condensers/evaporators that were cross-flow units. Entrance losses are expected to be higher in 4-port designs because the seawater flow is forced to abruptly change direction upon entering and to exit the module. In cross-flow units, the housings were designed to promote gradual entrances and exits. This explains why pressure drop in FL1 – FL3 is higher at the same Reynolds number compared to cross-flow units with smaller external channels (Figure 22). For similar external channel sizes, pressure drops in FL1 – FL3 are comparable to INT1 – INT7 SWAC units, which used a counter flow design with a custom housing.

Internal seawater pressure drop was lower in FL1 – FL3 compared to INT1 – INT7 for similar internal channel sizes (Figure 23). Makai previously observed the internal pressure drop in INT1 – INT7 was higher than expected and suggested a significant portion of the pressure loss occurred in the 55-mm manifolds used in the INT design. The FL design uses larger manifolds which have lower pressure drop for the same per plate flow rate.

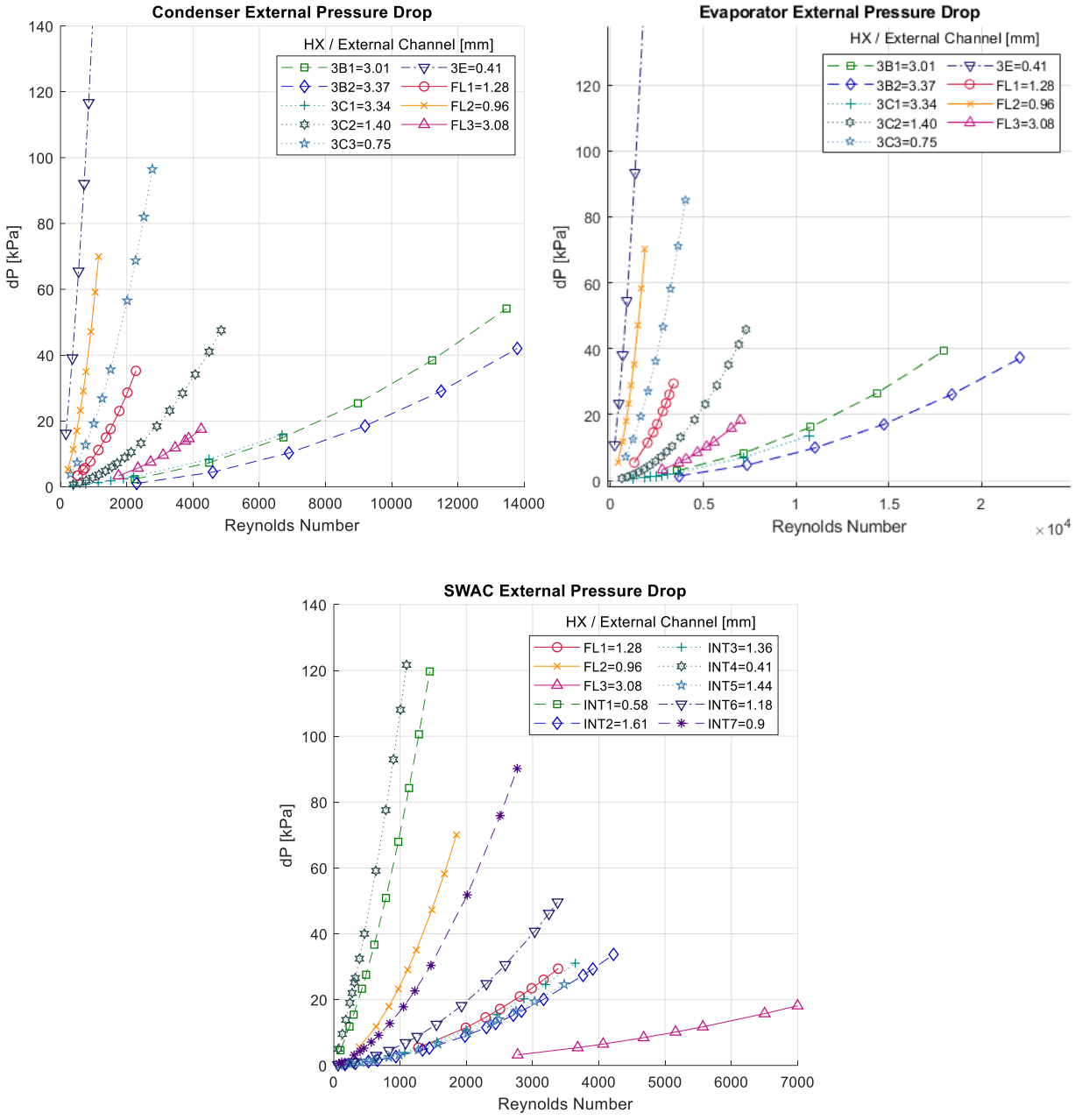

Figure 22. External seawater pressure drop comparison to previous TFHX designs.

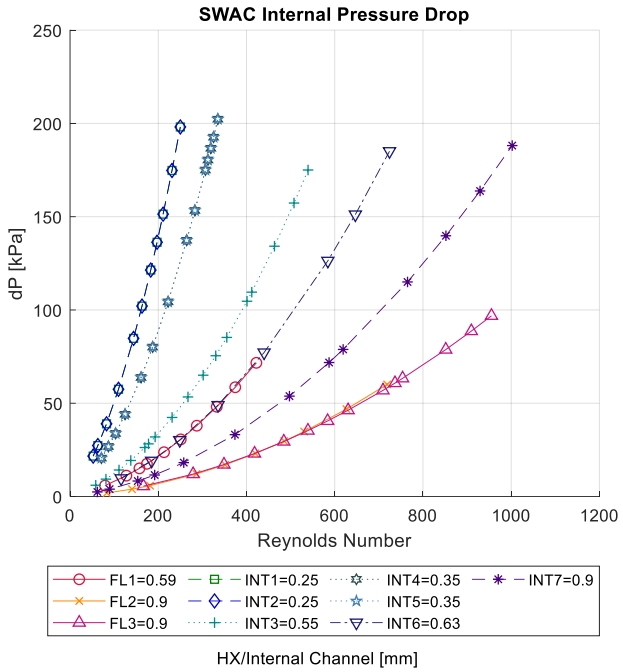

Figure 23. Internal seawater pressure drop compared to previous SWAC units.

5.1.2. Ammonia Pressure Drop

Ammonia-side pressure drop is an important consideration for an evaporator/condenser. In a closed-cycle OTEC system, minimizing the pressure drop increases the available differential pressure across a turbine and reduces the pumping power required to recirculate refrigerant. Ammonia pressure drop is strongly dependent on ammonia vapor flow rate, quality, and heat exchanger geometry.

The ammonia channels in FL1 are smaller than that of FL2 and FL3 (which are identical). As a condenser, the ammonia pressure drop in FL2 and FL3 are comparable and lower than the ammonia pressure drop in FL1. The pressure drop in all three condensers extrapolates to zero at zero duty (no flow).

As an evaporator, FL1 again has the highest pressure drop, but FL2 also has 30% higher pressure drop compared to FL3 at the same energy density. For all three units, the quality was maintained around 65%; quality variations do not account for the difference in pressure drop between FL2 and FL3. It is possible that for the same quality, the static head was greater in FL2. As shown in Section 5.1.4, the convective coefficients for FL2 and FL3 are in agreement; therefore, it is unlikely the channels were physically different or instrumentation errors (which would affect U-values used to calculate convective coefficients) were present.

In general, for the same ammonia mass flux, the normalized ammonia pressure drop is higher for smaller internal channels (Figure 25). Some variations are observed in evaporator testing with quality variations. An additional factor is the manifold and the transition zone designs for each TFHX type are different, so the pressure drop is not solely determined by the internal channel size.

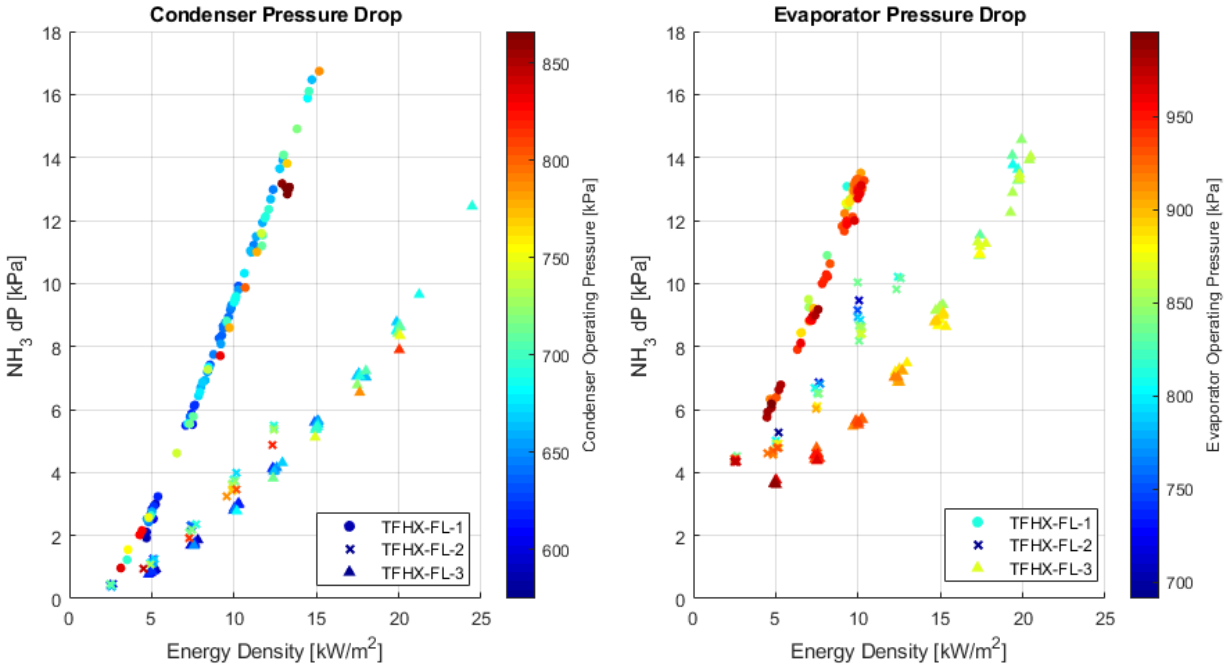

Figure 24. Ammonia-side pressure drop in condenser and evaporator mode.

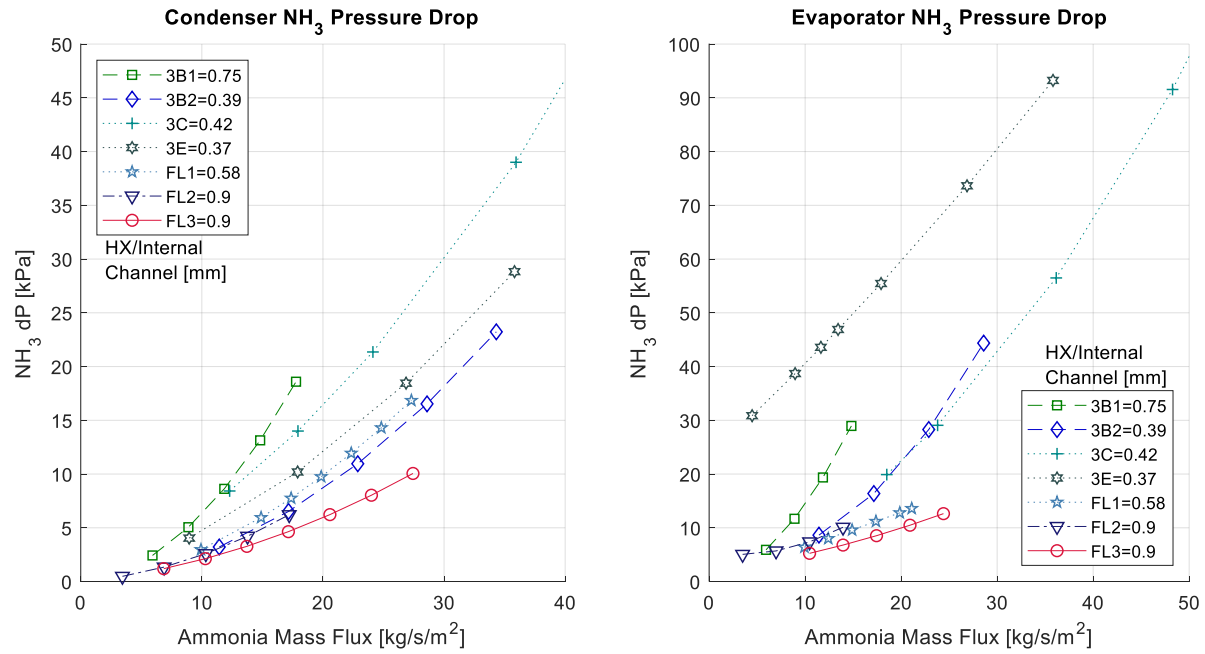

Figure 25. Comparison of ammonia-side pressure drop to previous TFHX units.

5.1.3. Overall Heat Transfer Coefficient

U-value is predominantly dependent on seawater flow rate but duty (and quality for an evaporator) also have an effect. In both condenser and evaporator modes, U-value increases logarithmically with increasing seawater Reynolds number (Figure 26). As a condenser, for the same seawater

Reynolds number, U-value decreases <10% with increasing energy density. As an evaporator, for the same seawater Reynolds number, U-value increases < 10% with increasing energy density. In evaporator mode, decreasing quality from 90% to 50% increases U-value ~ 10% (Figure 27).

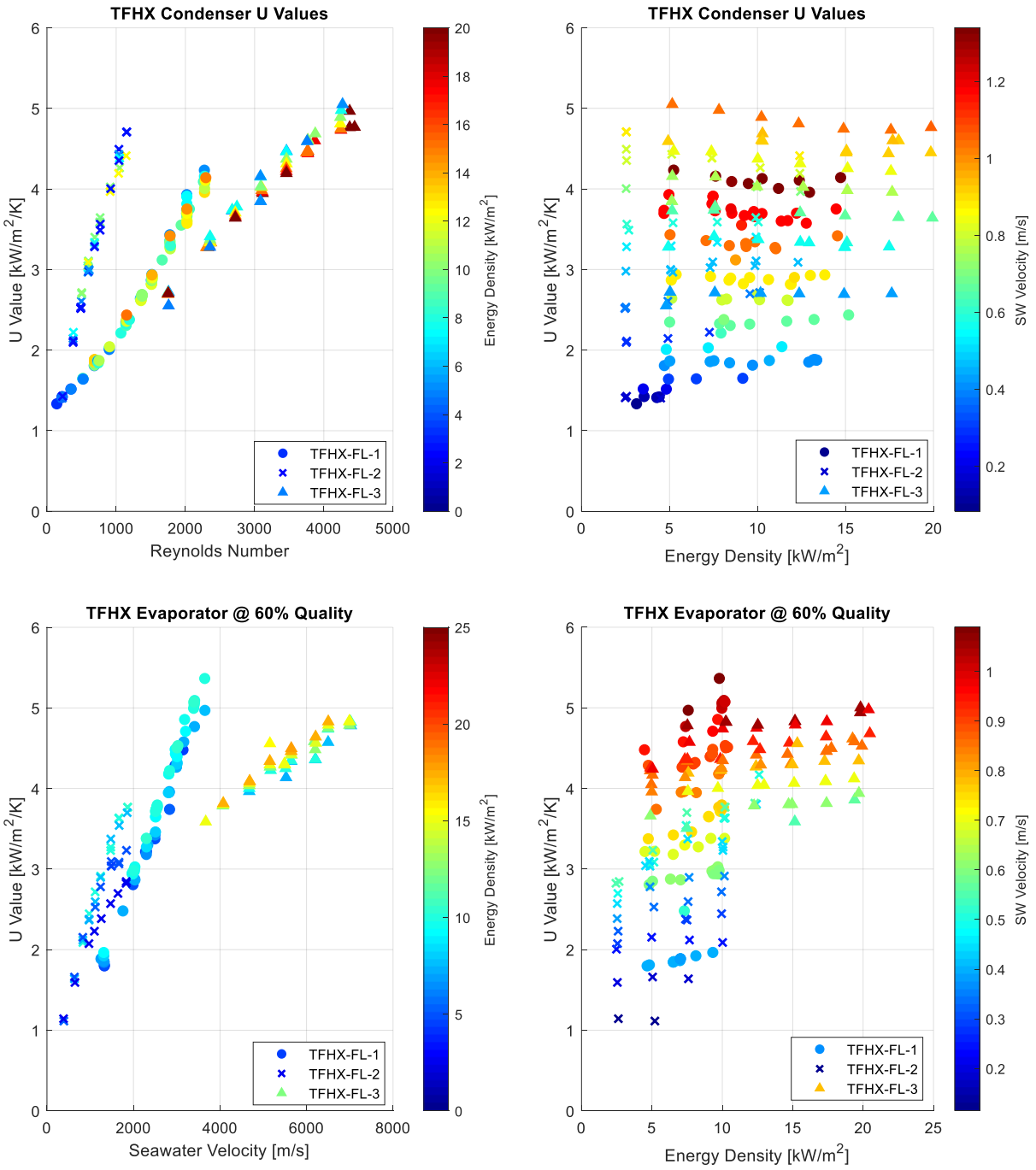

Figure 26. Effect of seawater velocity and energy density on U-value for TFHX units in condenser and evaporator mode.

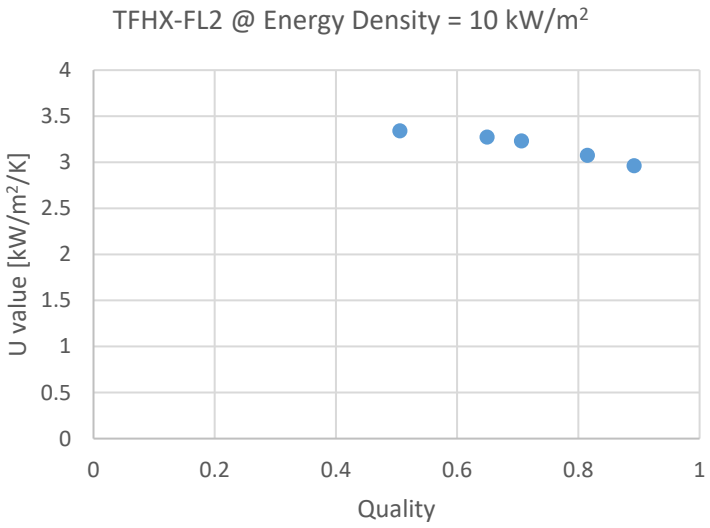

Figure 27. Effect of quality on U-value.

To account for the different seawater channel sizes, seawater flow rates, and seawater pressure drops, U-values for each TFHX unit is better compared when plotted against seawater pumping power (Figure 28). As a condenser, for the same pumping power, FL3 has 25-33% higher U value compared to FL2 and FL1, across all energy densities. As an evaporator, there is more U-value variation with energy density and the distinction between the three TFHXs is less pronounced, but FL3 still has higher U values for the same pumping power.

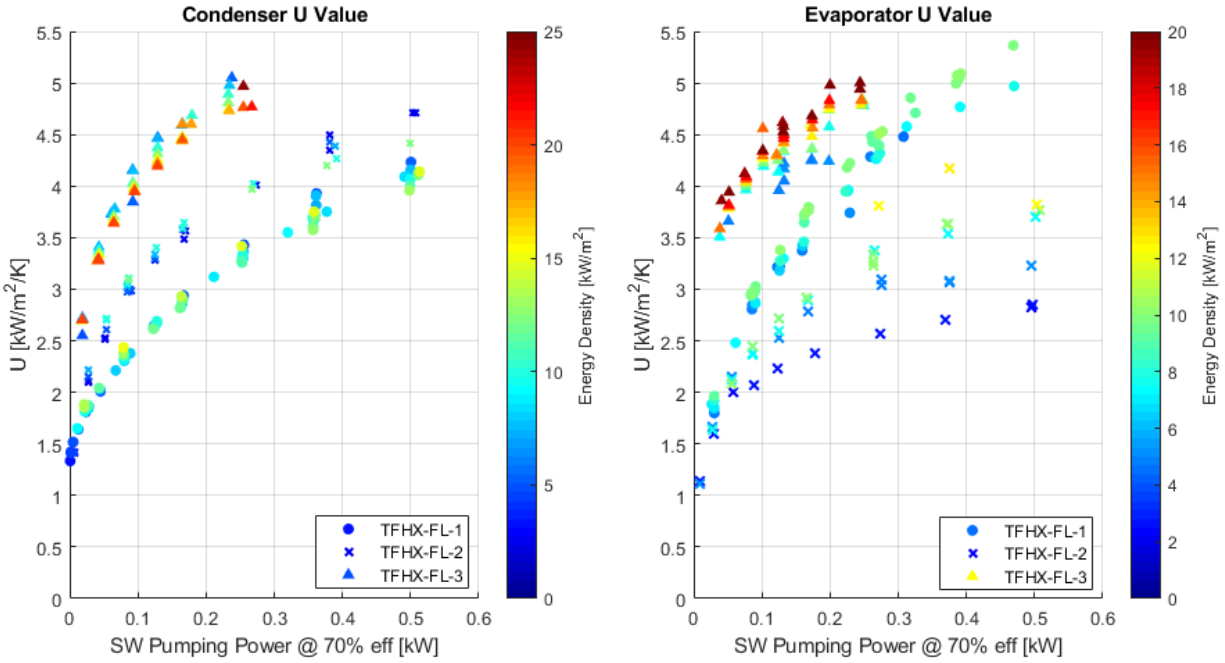

Figure 28. U-value versus seawater pumping power for different energy densities.

To compare the TFHX FL units with previous TFHX designs and previously tested 2MW heat exchangers, the U-values must be compared versus pumping for the same duty at the same energy density. TFHX designs had comparable U-values to previously tested 2MW heat exchangers. As a condenser, larger seawater channels and larger ammonia channels had higher overall U-values for the same pumping power. As an evaporator, designs with smaller ammonia channels have higher U-values; there was no clear trend on seawater channel size.

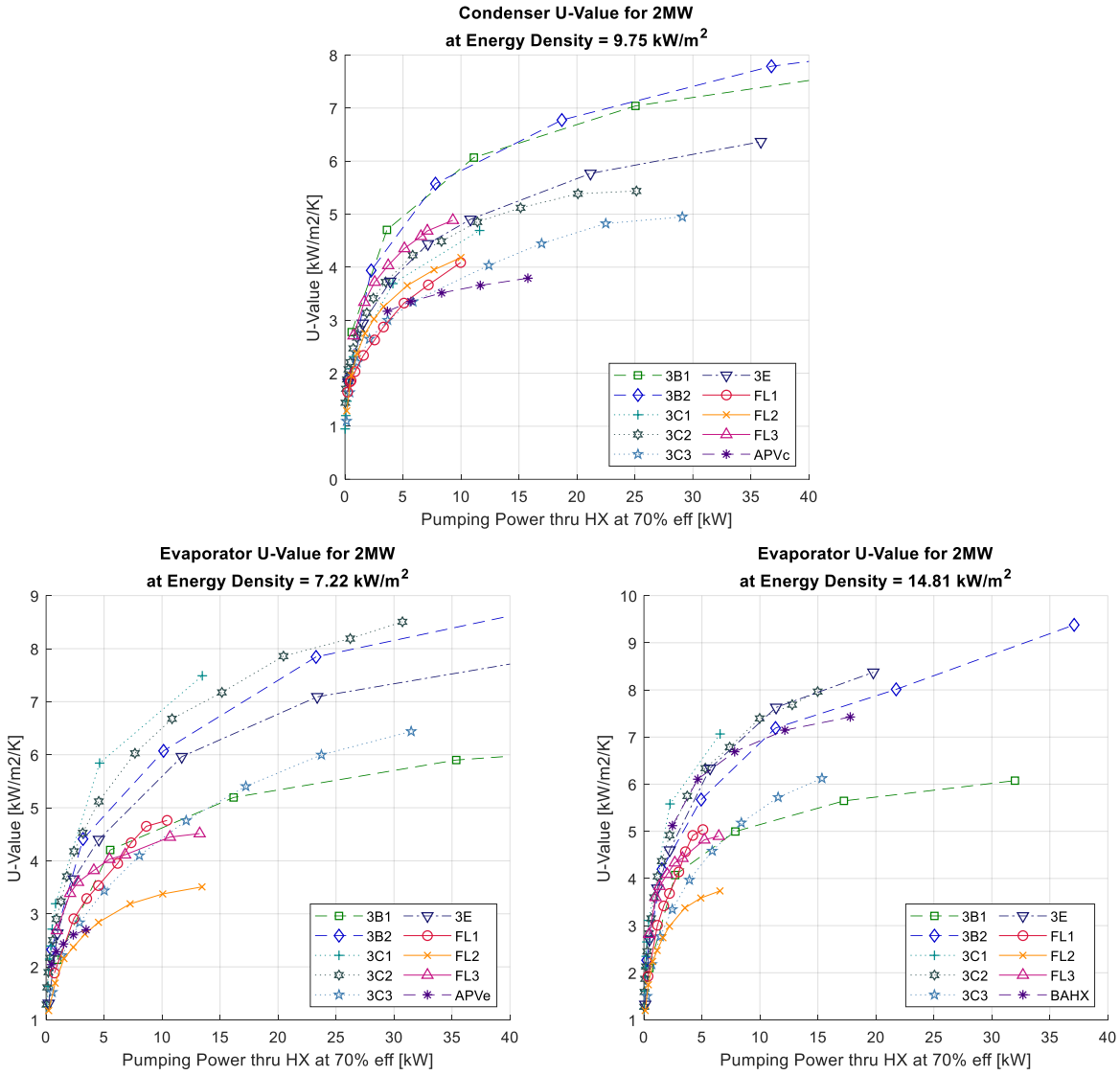

Figure 29. Comparison of U-value vs pumping power with TFHX units scaled to 2MW duty at the same energy density as other 2MW heat exchangers.

In SWAC testing, U-Value is primarily dependent on external seawater flow rate, although for the same external flow rate, up to 33% difference in U-value was observed between minimum and maximum internal flow rates (Figure 30). As in condenser and evaporator testing, U-value is also plotted versus pumping power to account for channel size and pressure drop differences. At the same external pumping power and comparable internal pumping power, FL3 has U-value nearly 2X FL2 and 20% higher than FL1.

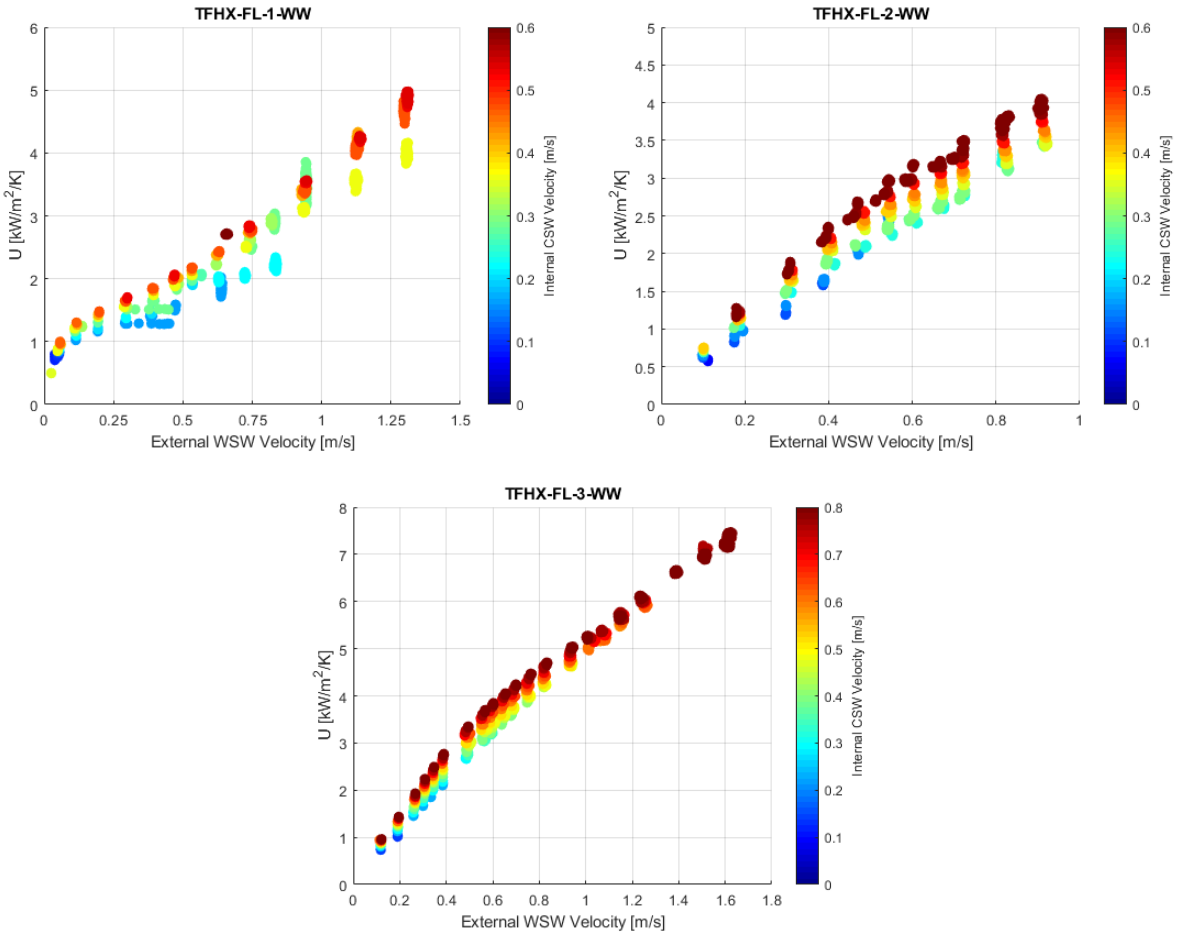

Figure 30. SWAC testing U-values.

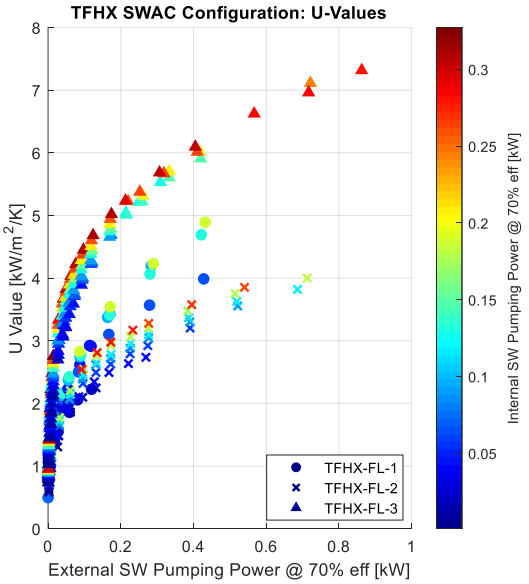

Figure 31. U-value versus Reynolds number and pumping power in SWAC testing.

5.1.4. Ammonia Convective Coefficients

Ammonia convective coefficients were calculated for each TFHX using a constrained least-squares solver, where the lower bound for the convective coefficients is 0.

Ammonia-side convective coefficients for FL2 and FL3 are in agreement. Compared to FL2 and FL3, FL1 has lower convective coefficients as a condenser but higher as an evaporator. The smaller channels in FL1 may have encouraged vapor shear as an evaporator to improve convection but may not have passed condensed ammonia quickly enough as a condenser and led to lower convective coefficients.

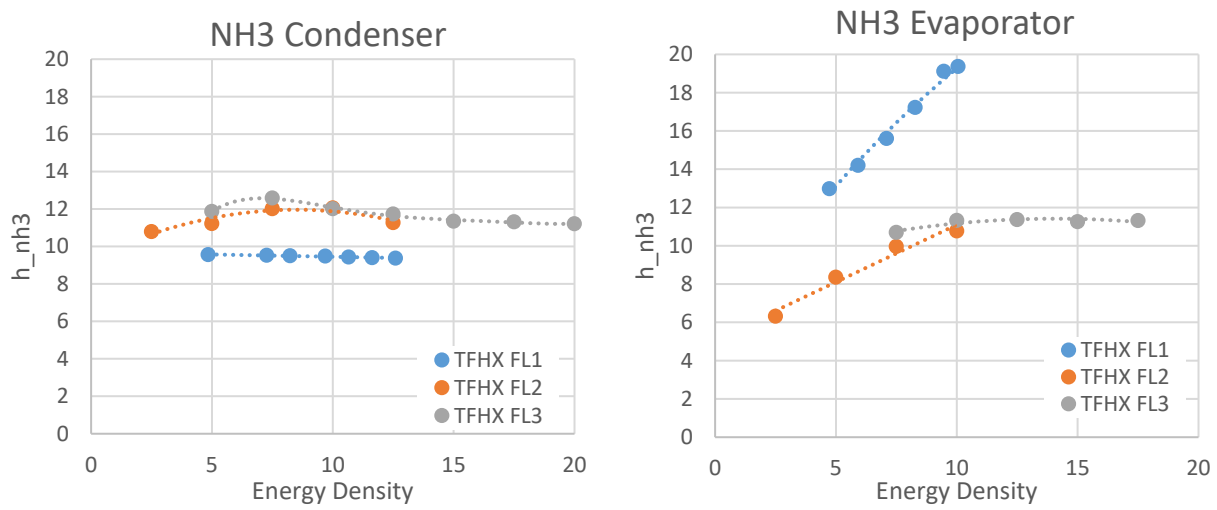

Figure 32. Ammonia-side convective coefficients for condenser and evaporator.

Compared to previous TFHXs, for the same mass flux (ammonia vapor flow rate divided by ammonia cross sectional flow area), in a condenser the ammonia convective coefficient is larger for larger internal channels and shorter flow paths. In an evaporator, smaller channels improved the ammonia convective coefficient at lower mass fluxes. Designs with larger channels and longer flow paths had increasing ammonia convective coefficients with increasing mass flux. For the same energy density, TFHX designs had comparable or higher ammonia convective coefficients compared to 2MW APV and BAHX heat exchangers.

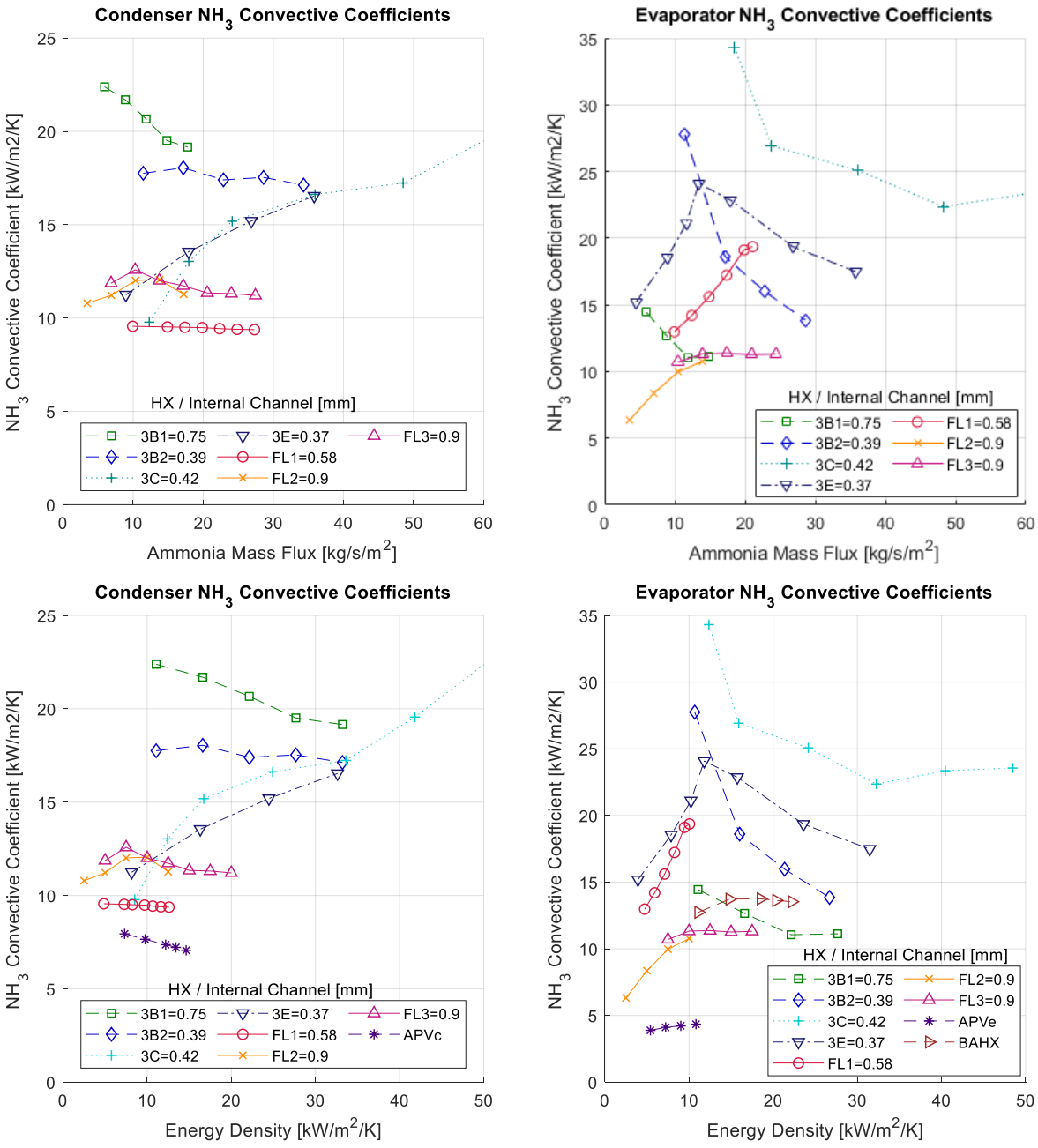

Figure 33. Comparison of ammonia convective coefficients with previous heat exchangers.

5.1.5. Seawater Convective Coefficients

Seawater side convective coefficients were solved independently for each configuration (condenser, evaporator, and SWAC) for each TFHX unit. For each unit, all three configurations produced external seawater convective coefficients that are in agreement (Figure 34). As in previous results, seawater convective coefficients increase almost linearly with increasing seawater velocity.

In previous results, larger channels had higher convective coefficients at the same velocities. In this round of testing, FL1, which had a larger channel than FL2, had a lower convective coefficient (Figure 35). FL3, which had a seawater channel nearly 3X that of FL2 had convective coefficients < 15% higher than FL2 at the same velocities.

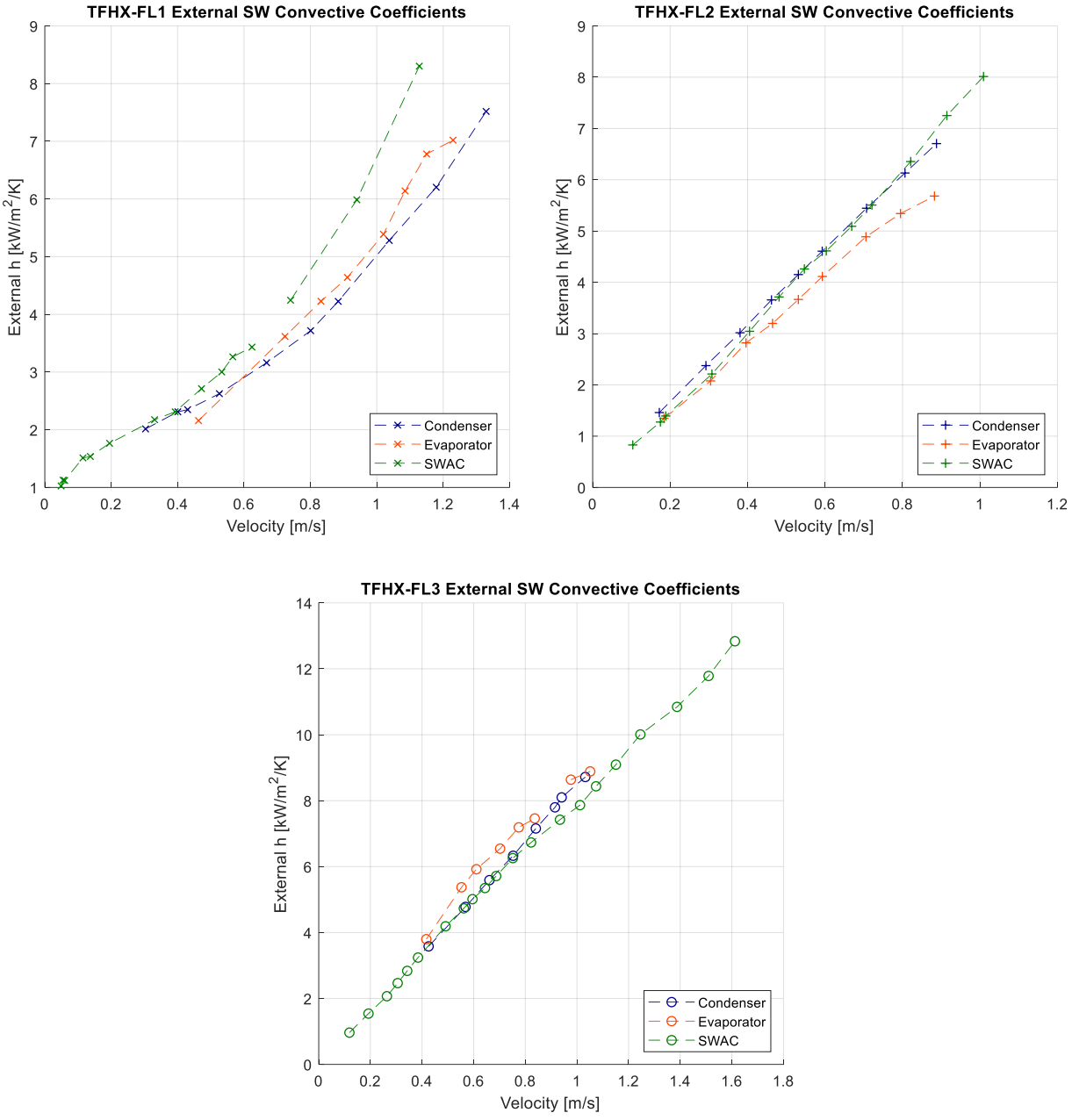

Figure 34. Seawater-side convective coefficients calculated individually for each configuration showed strong agreement.

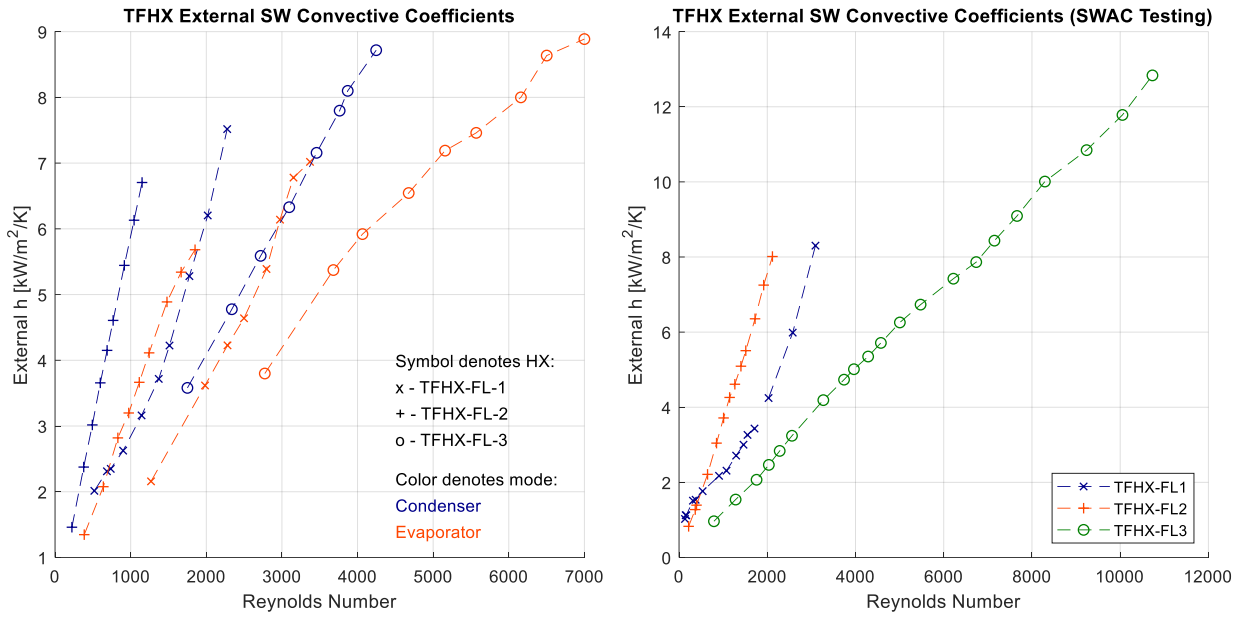

Figure 35. At the same Reynolds number, the smaller channel in FL2 had higher convective coefficients.

In order to compare against other TFHX designs and previously tested 2MW heat exchangers, data must be normalized to a duty and energy density (Figure 36). For condenser comparisons, data were normalized to the 2MW APV heat exchanger at an energy density of 9.75 kW/m^2. For evaporator comparisons, data were normalized to both the 2MW APV heat exchanger at an energy density of 7.22 kW/m^2 and the 2MW BAHX heat exchanger at an energy density of 14.81 kW/m^2. For the same pumping power, larger channels have higher seawater convective coefficients. One exception was TFHX-3E, which had the smallest seawater channel and a short path length. For the same pressure drop, the volumetric flow rate was 5X less in 3E compared to TFHXs with 3mm channels; the lower volumetric flow rate balances the high pressure drop and the pumping power is comparable to that in TFHXs with larger channels. Overall, TFHX designs had comparable seawater convective coefficients compared to both APV heat exchangers but lower seawater convective coefficients compared to the BAHX heat exchanger.

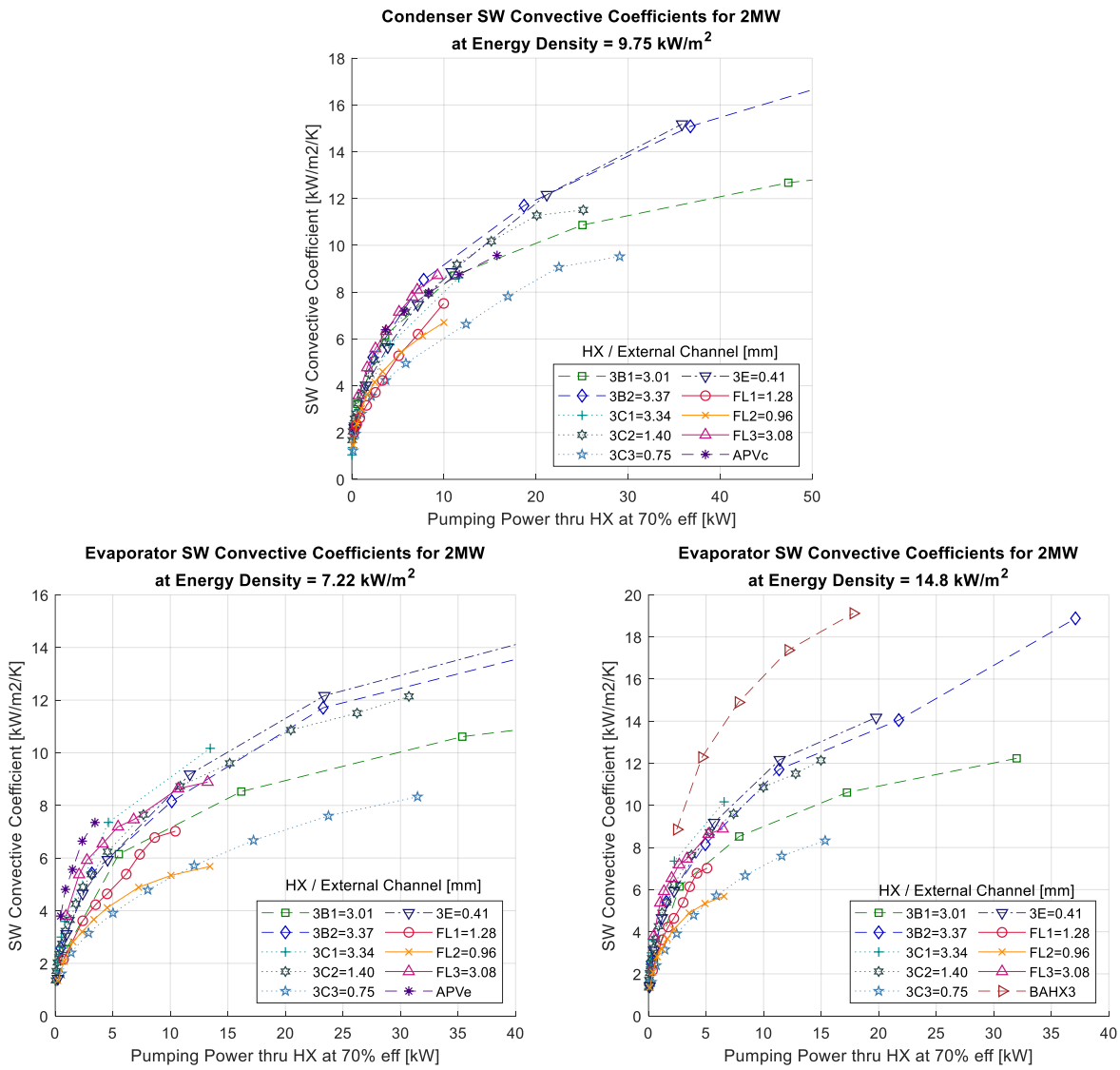

Figure 36. Comparison of external seawater convective coefficients versus pumping power through the heat exchanger. TFHXs are scaled up to a 2MW unit at the same energy density as previously tested APV or BAHX heat exchangers.

The internal seawater convective coefficients in SWAC testing are shown in Figure 37. There is discrepancy in the internal convective coefficients of FL2 and FL3; FL2 is lower by up to 25% when, because the channels are the same, the convective coefficients should be comparable, as observed in the ammonia convective coefficients during condenser and evaporator testing.

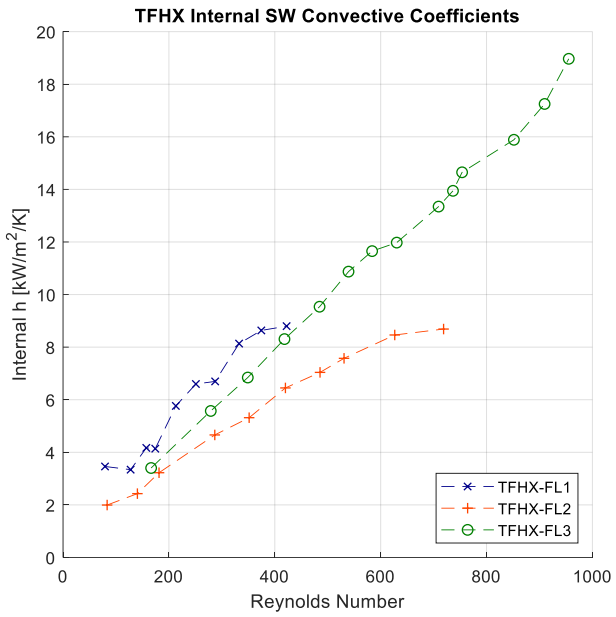

Figure 37. Internal seawater convective coefficients from SWAC testing.

Compared to previous testing, the internal convective coefficients for FL1 and FL2 are comparable to WW-INT5/6 and WW-INT7 which had similar internal channel sizes (0.55mm/0.62mm, and 0.9mm, respectively, Figure 38). FL3, which has the same internal channel size as FL2 and INT7 had significantly higher internal convective coefficients.

The reasons for the convective coefficient discrepancies is unclear. One possibility is that by removing the external channel spacers and trimming the plates introduced uneven external channel spacings or poor flow distribution. Analysis methods assume uniform energy density and can affect results when the assumptions are invalid.

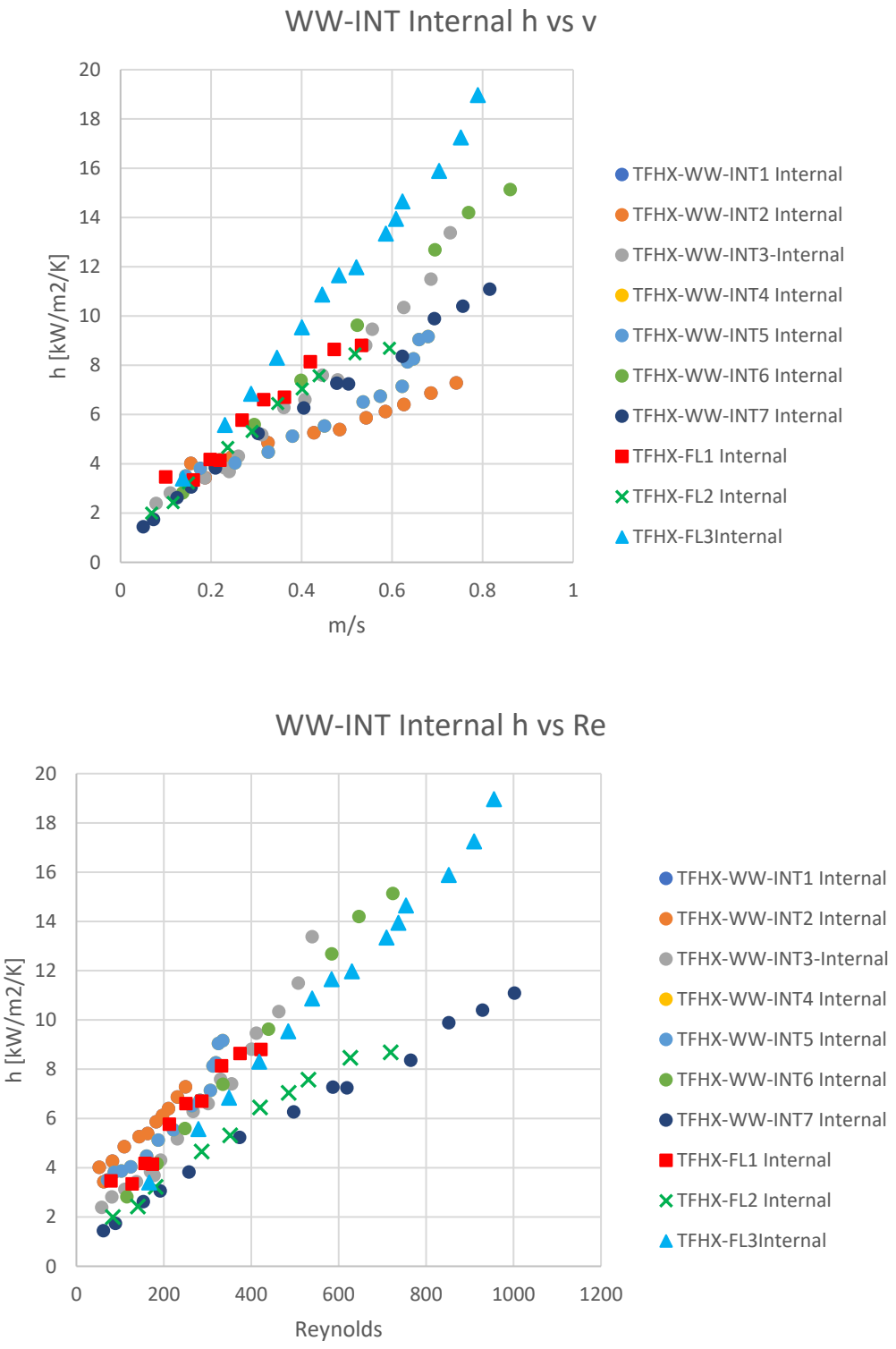

Figure 38. Internal convective coefficient comparison with previous SWAC testing results.

5.1.6. Heat Exchanger Operating Pressure

Ammonia-side operating pressure is determined by the seawater temperature, seawater flow rate, duty, and quality (for an evaporator). Makai previously reported for each heat exchanger design at a fixed seawater flow rate and duty (and quality), the operating pressure can be predicted based on a fixed offset from the ammonia saturation curve for the seawater temperature. Attaining an operating pressure as close as possible to the saturation pressure corresponding to the seawater inlet pressure maximizes the pressure drop across a turbine, and, therefore, gross power. Higher seawater flow rates yield operating pressures closer to the seawater temperature, but also require higher parasitic losses from high volumetric flow rates and/or high seawater pressure drops.

One way to compare heat exchanger performance is to compare heat exchanger operating pressure versus energy density at fixed pumping powers (Figure 39 and Figure 40). In both condenser and evaporator modes, FL2 had the least optimal ammonia-side pressure for the same seawater pumping power. FL3 had the lowest condenser pressure and highest evaporator pressure (i.e., maximum turbine differential pressure) for the same seawater pumping power. However, it is also important to consider the overall seawater flow rate. TFHX-FL3 had wide channel spacings and more seawater flow was available for the same heat exchanger pumping power. This analysis does not account for the effects of increased seawater flow rates on the rest of an OTEC system. For a fixed OTEC system size, higher seawater flow rates lead to higher parasitic losses in the system. Alternatively, higher seawater flow rates may require larger, more costly systems (i.e., larger cold water pipe). The system effects and economics must also be considered when evaluating heat exchangers for an OTEC system.

Makai developed a program to utilize empirical data to assess the thermo-hydraulic performance of different heat exchangers in an OTEC system (Section 5.1.7).

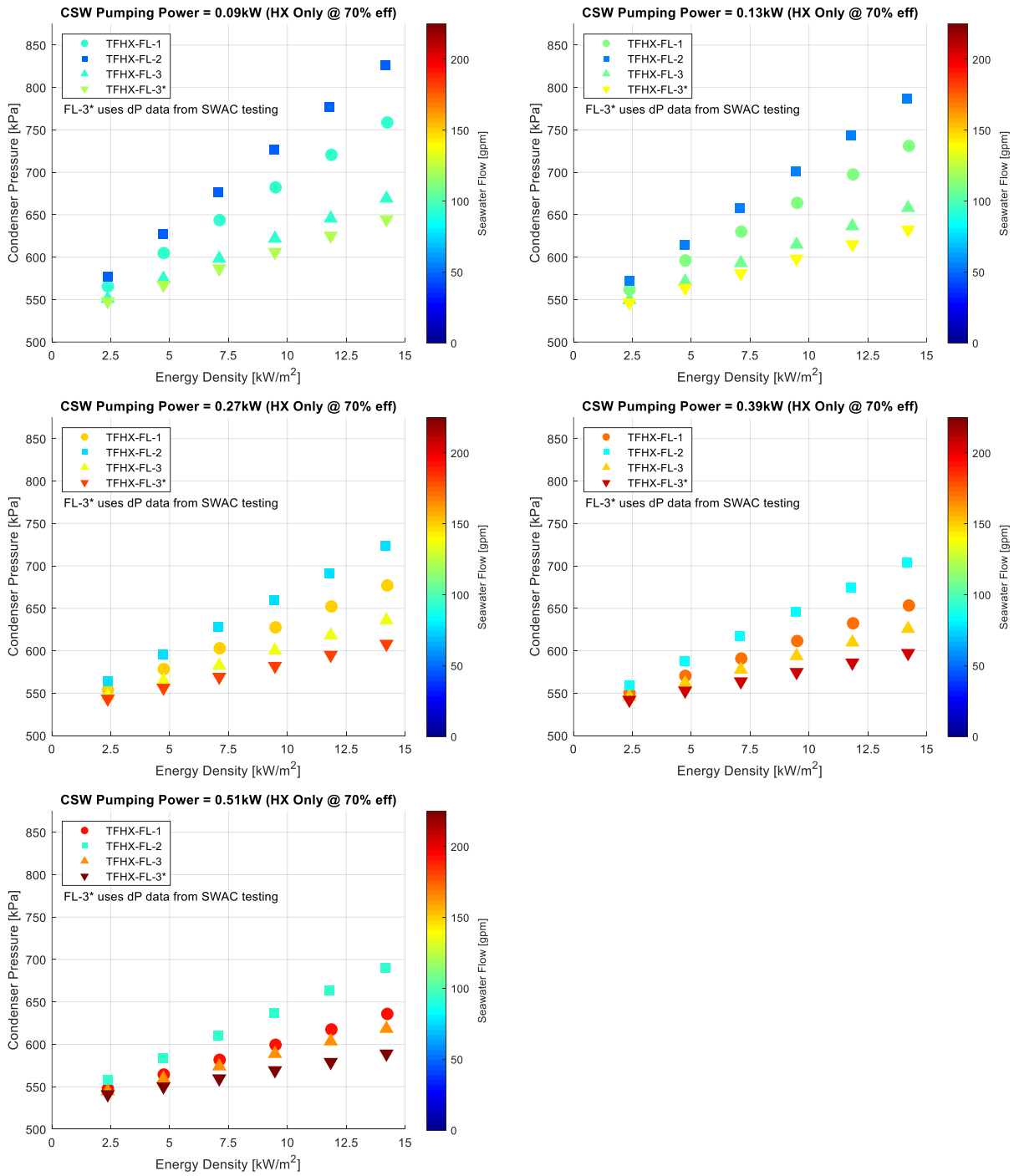

Figure 39. Comparison of condenser operating pressure versus energy density for cold seawater temperature = 6°C at different seawater pumping powers (through the heat exchanger only).

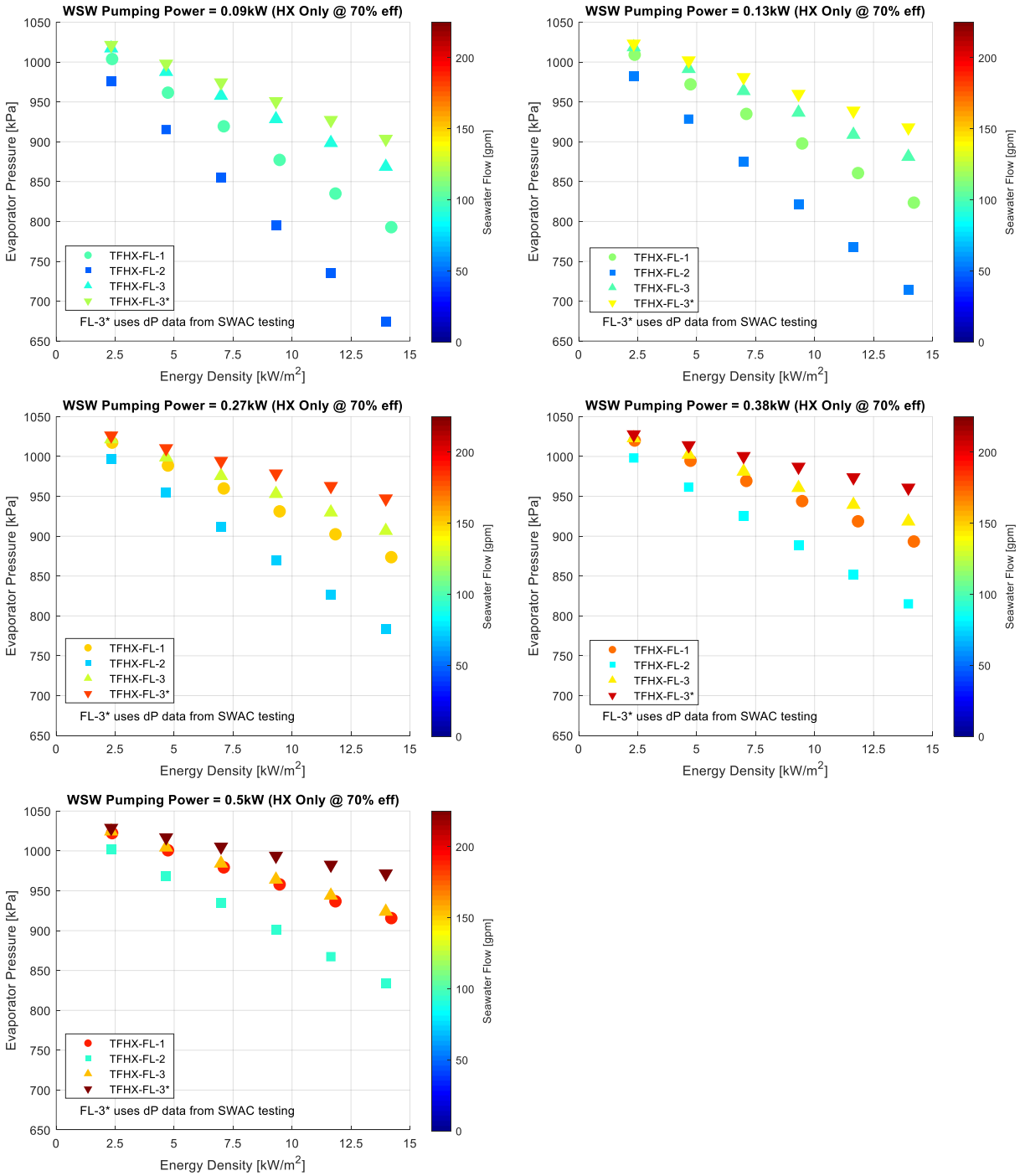

Figure 40. Comparison of evaporator operating pressure versus energy density for warm seawater temperature = 26.5°C at different seawater pumping powers (through the heat exchanger only).

5.1.7. Effectiveness

Another consideration in the design of heat exchangers is the effectiveness, the actual heat transferred compared to the maximum possible heat transfer. For a seawater-cooled heat exchanger, the most effective design would meet duty and pumping power (pressure drop) requirements while extracting as much cooling capacity from the cold seawater as possible.

Differences in internal/external channel size affect both pumping power and effectiveness (Figure 41). The smaller internal channels in FL1 resulted in high effectiveness but may require more area to meet duty requirements. Larger channel spacings can provide more duty at the same pumping power (because the pressure drop is lower), but at lower effectiveness.

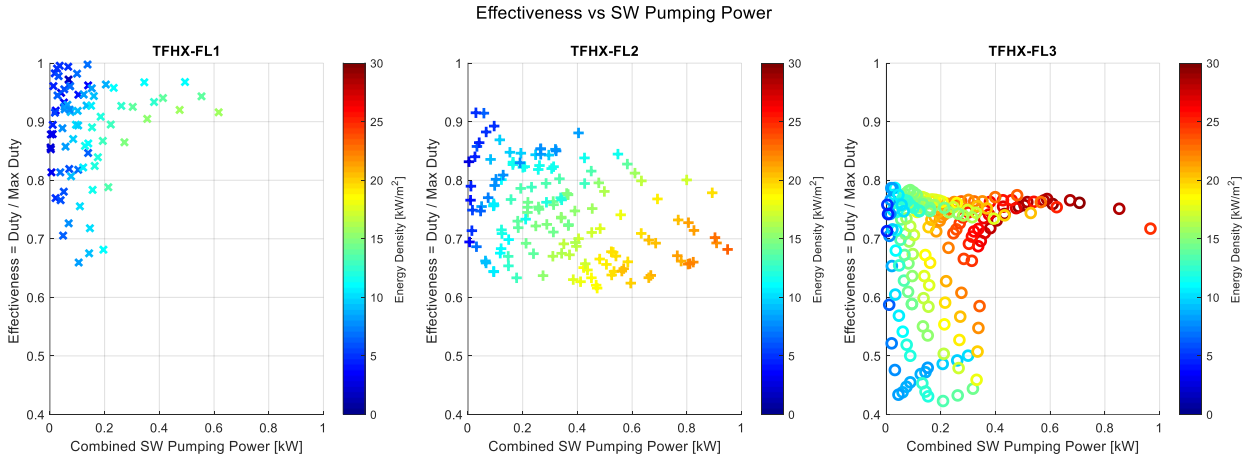

Figure 41. Effectiveness depends on duty and seawater pumping power.

5.2. DISCUSSION

5.2.1. Compactness

TFHXs contain more heat transfer area per cubic meter (m^2/m^3) than plate-and-frame, brazed fin, and shell-and-tube heat exchangers (Figure 42). FL1 and FL3 are in the same range of compactness compared to previous TFHX designs. At the same energy density, TFHXs require less than 25% of the volume of previously tested heat exchangers to produce the same duty (Figure 43).

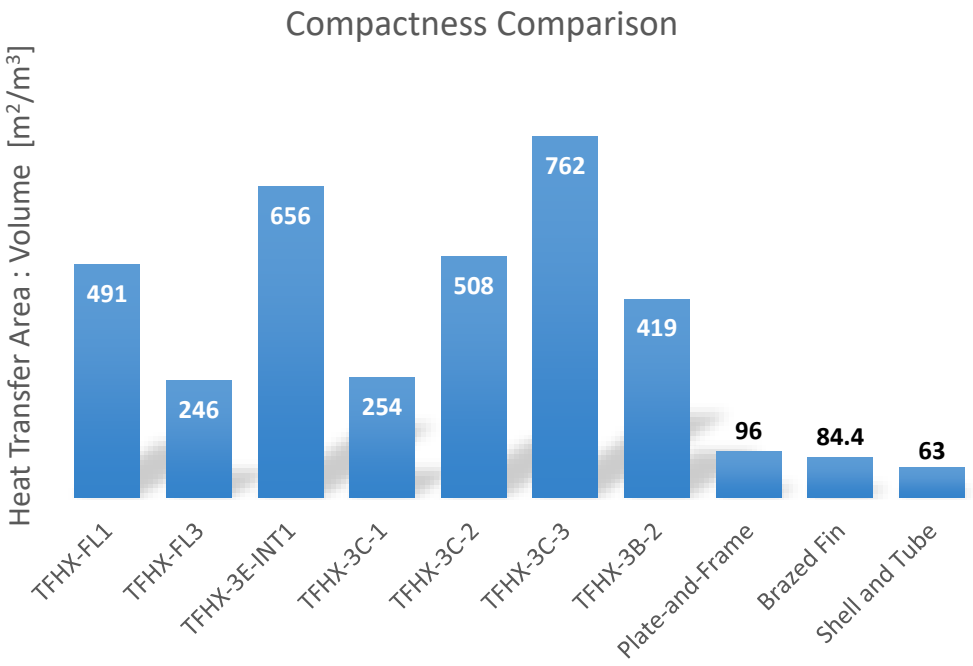

Figure 42. TFHX heat exchangers have more heat transfer area per volume compared to the previously tested plate-frame (APV), brazed fin (BAHX3), and shell and tube (ETHX) heat exchangers

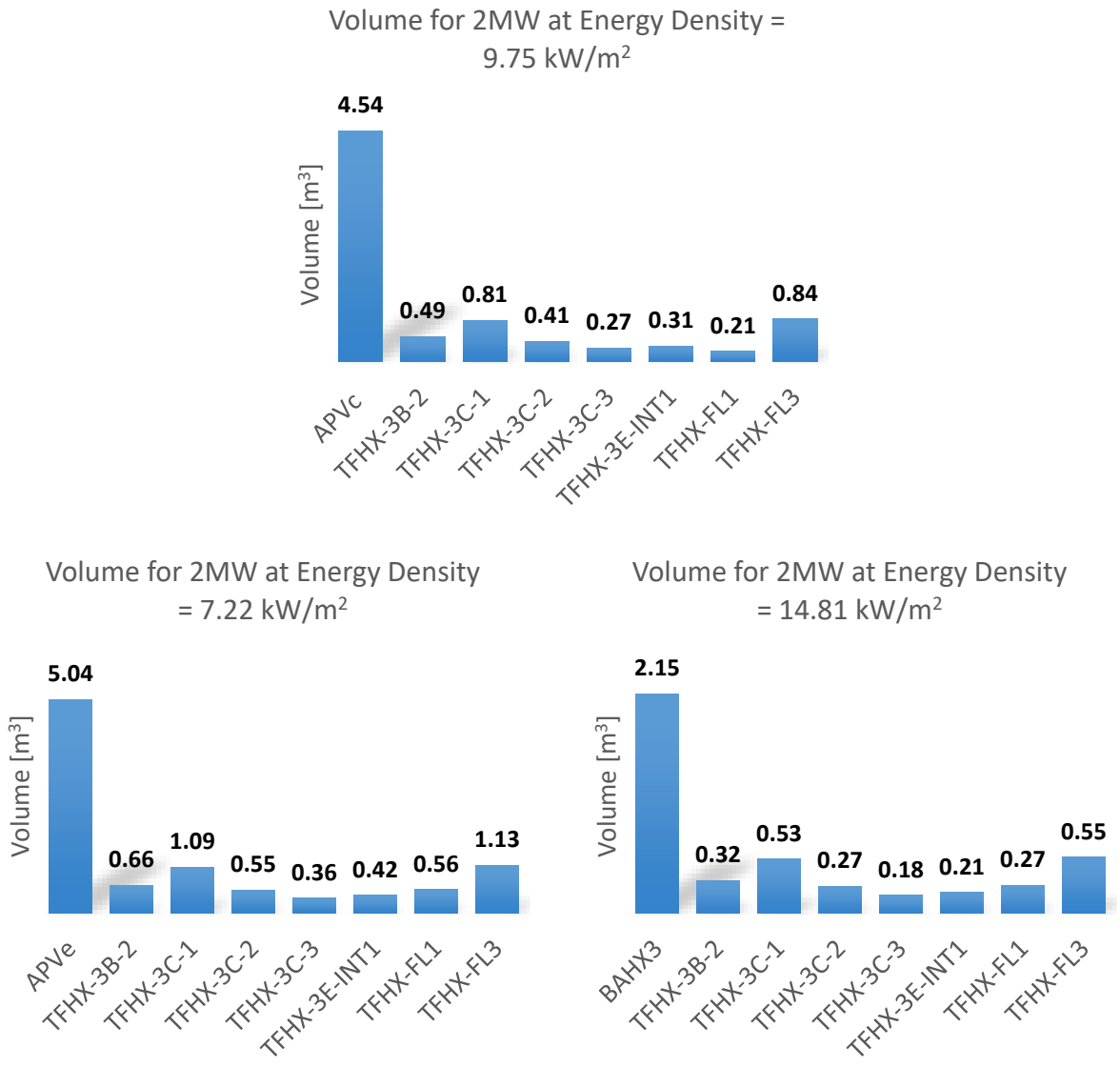

Figure 43. Comparison of volume required for 2MW of duty at various energy densities. Energy density was selected to match previously tested heat exchangers.

5.2.1. OTEC Heat Exchanger Design

Makai developed an OTEC Power Calculator as a tool to evaluate different heat exchanger designs in the context of an OTEC system. Heat exchangers can be compared in terms of area (i.e., heat exchanger cost) or volume (i.e., system size and cost) required to produce a targeted net power.

In this analysis, to provide comparison between heat exchanger designs, the cold water pipe size and seawater flow rates is fixed. For each heat exchanger design, heat exchanger area and turbine characteristics are adjusted to maximize the average annual net power (Figure 44).

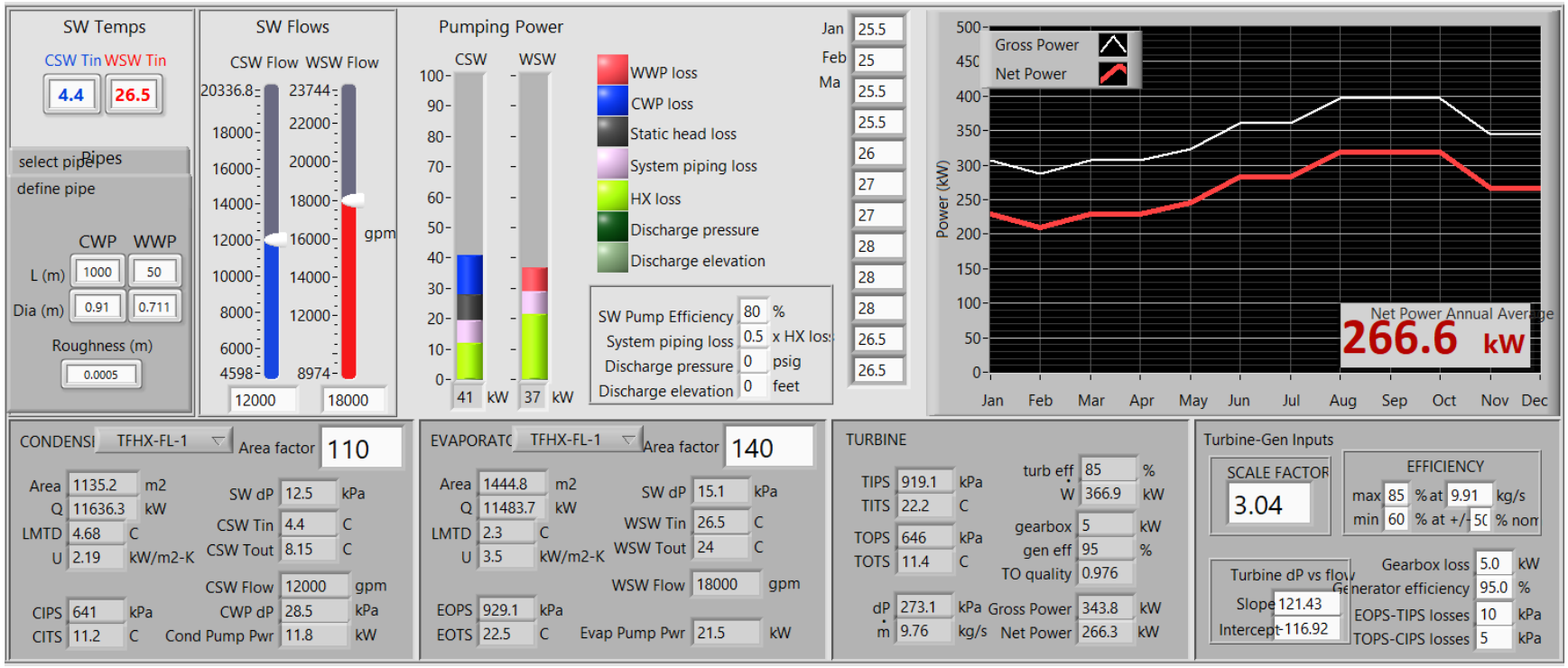

Figure 44. Screenshot of OTEC Power Calculator using TFHX FL1.

At a fixed cold seawater flow rate of 12,000 gpm and a warm seawater flow rate of 18,000 gpm, different combinations of condenser and evaporator areas for TFHX-FL1, Fl2, FL3, and APV were evaluated for the average annual net power produced (Figure 45). For the same seawater flow rates and total heat exchanger area (up to 6,000 m^2), all four heat exchanger designs produced comparable net power. In TFHX, increasing heat exchanger area yielded diminishing returns in net power. With fixed seawater flow rates, continuing to add APV heat exchanger area results in the most net power. However, since the cost of an OTEC system is proportional to heat exchanger area (heat exchanger cost) and heat exchanger volume (structural cost), net power should be compared in the context of the required heat exchanger area and volume (Figure 46). For the same heat exchanger area, TFHX-FL1 and FL2 have over 4X more net power density compared to APV heat exchangers.

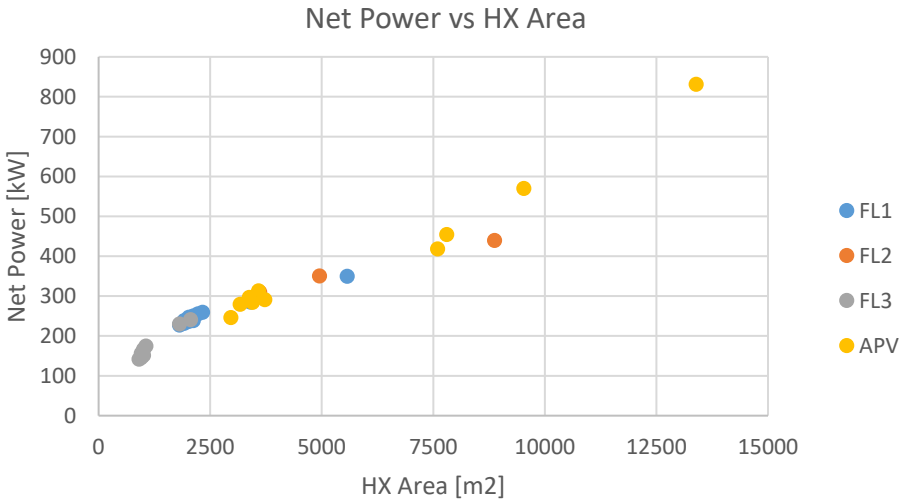

Figure 45. Net power vs HX area for fixed cold and warm seawater flow rates.

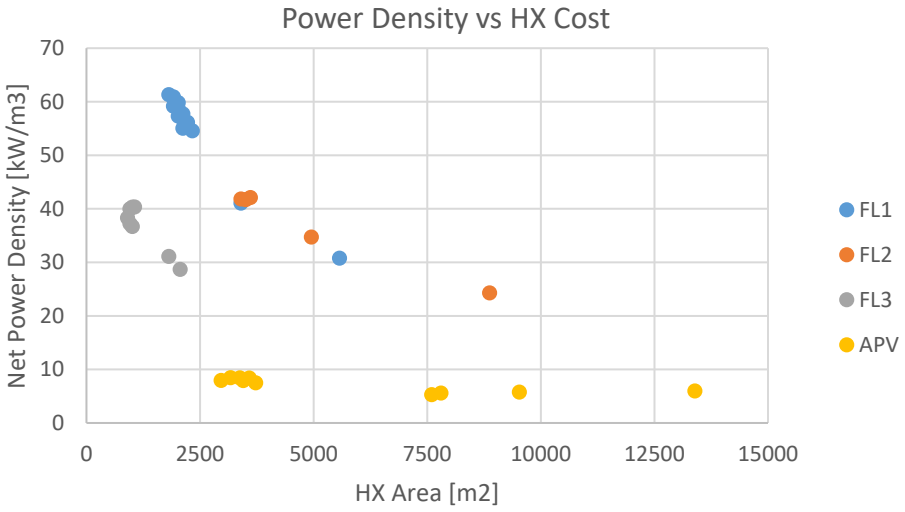

Figure 46. Net power density versus heat exchanger area for a fixed cold water pipe size and seawater flow rates.

5.2.2. SWAC Heat Exchanger Design

Makai previously contacted HECO regarding an auxiliary cooling application where warm seawater was used to cool a freshwater loop. HECO provided specifications for hot and cold fluid flow rates, temperatures, and pressure drops.

Of the tested FL designs, TFHX-FL2 best fit the HECO operating conditions; however, the FL2 design requires over 2.5X the area of the existing heat exchanger to meet the internal pressure drop requirements while providing only 10% increase in duty. Another option is to use shorter TFHX plates and increase the seawater flow; in this scenario, TFHX area would be comparable to the existing heat exchanger, the hot water flow conditions remain the same, but the seawater flow rate is increased by 800 gpm. Both hot water and seawater pumping powers through the TFHX are lower than the specification, but due to the increased seawater flow rate, the increased pressure drop through the seawater system must also be considered (Makai was not provided system design information).

Table 4. TFHX designs for HECO conditions

	HECO Specs	FL2, match hot dP	shorter plate, increase cold side flow	
Area	317.32	814.86	342.96	**m^2**
Duty	6514.38	7304.97	6546.54	**kW**
Hot Water Flow Rate	3000	3000	3000	**gpm**
Hot Water T in	41.67	41.67	41.67	**°C**
Hot Water T out	33.39	32.36	33.32	**°C**
Hot Water dP	3.96	3.50	3.43	**psi**
Hot Water Pumping Power (70% eff)	7.38	6.52	6.38	**kW**
Cold Water Flow Rate	3000	3000	3800	**gpm**
Cold Water Tin	27.78	27.78	27.78	**°C**
Cold Water T out	36.19	37.20	34.45	**°C**
Cold Water dP	3.99	1.96	2.62	**psi**
Cold Water Pumping Power (70% eff)	7.44	3.54	6.01	**kW**

This case study reiterated a common finding Makai has encountered when approached with direct-replacement applications for the TFHX. Because the TFHX is a fundamentally different heat exchanger and existing heating/cooling systems are designed to operate with conventional heat exchangers, directly replacing a conventional heat exchanger with a TFHX does not leverage TFHX performance advantages. In these applications, TFHXs must be competitive on an economic, ease of maintenance, or durability/lifetime basis.

5.3. BIOFOULING TESTING

In March 2022, Makai began a biofouling test using TFHX-FL1. The goal of the test is to determine how pressure drop and U-value are affected by fouling and to determine whether cleaning methods are required to maintain performance.

5.3.1. Biofouling Station

A biofouling test station (Figure 47) was constructed to run two independent test units. Each station uses a separate warm seawater supply (with a separate strainer). The cold seawater supply from a common line and both units share a common drain. Different strainers will be tested to determine what mesh size is sufficient to prevent larger objects from clogging the external channels.

During testing, the module will have cold seawater flowing in the internal channels and warm seawater in the external channels. Fouling is not expected on the cold seawater side, but flowing cold seawater, rather than maintaining a stagnant, pressurized channel, enables U-value monitoring.

Figure 47. Biofouling test station.

A data acquisition system to collect temperature, pressure, and flow measurements was built for the biofouling test. Inlet and outlet temperatures and pressures for both cold (internal) and warm (external) seawater flows are measured. Only warm seawater flow is measured; cold seawater flow rate is calculated using a duty balance. A custom Labview-based monitoring program was developed to record and display performance data.

For this first test, a strainer with 1/32" (0.8 mm) mesh size was used. The effective external channel spacing on FL1 was 1.2mm; any particles that pass through the strainer should also pass through the heat exchangers. The target warm seawater flow rate was 100 gpm, which corresponds to a velocity of 0.75 m/s and 10 kPa (1.5 psi) pressure drop. Because the seawater control valves are manually positioned, seawater flow varies with: 1) NELHA supply pressure, 2) pressure drop across the strainer, and 3) pressure drop changes in the test unit from biofouling or clogging.

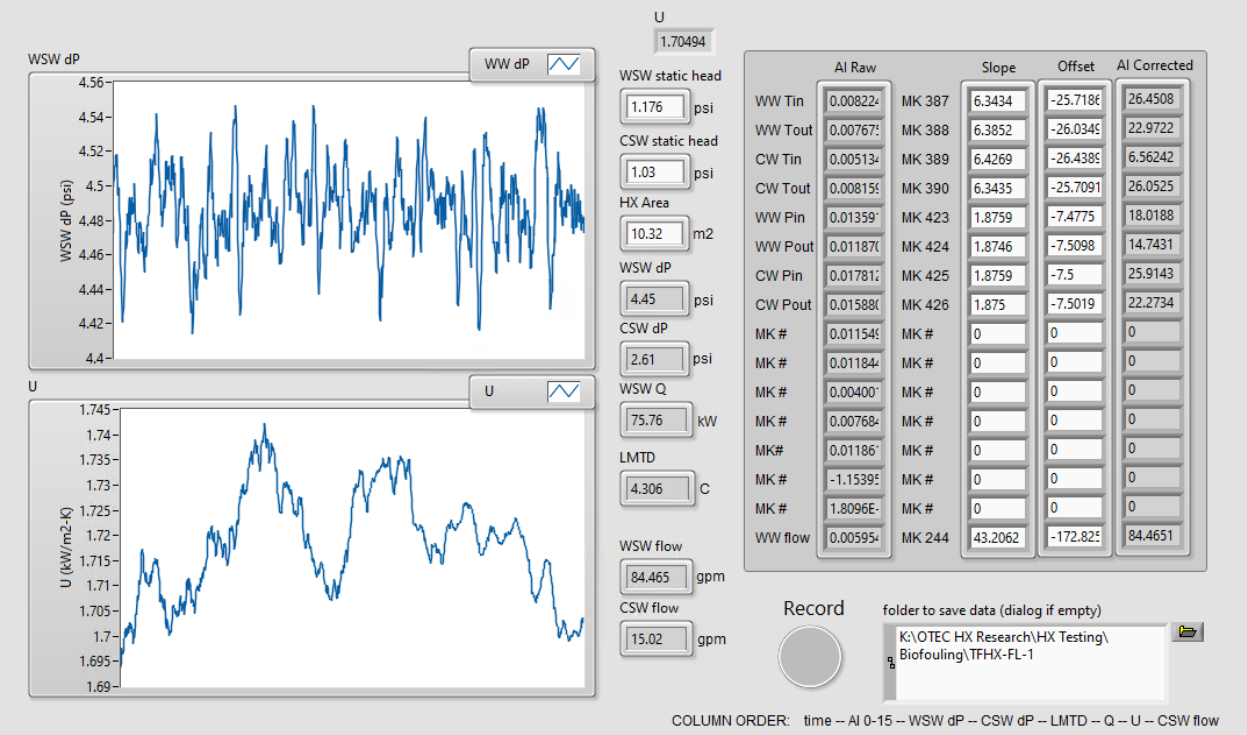

Figure 48. Biofouling performance monitoring program.

5.3.2. Biofouling Results

In this first test, to establish a baseline for biofouling performance, the strainer and the inlet/outlet ports of the TFHX unit were inspected and cleaned by spraying with water every 30 days (Figure 51). No chemicals, plate disassembly/assembly, or reverse circulation cleaning methods were used. In addition to visual inspections, a baseline pressure drop vs flow test and U-value vs flow was conducted after FL1 was installed in the Biofouling Test Station for performance data comparison.

Pressure drop has increased over 2X over the duration of the test (Figure 49). Initially, pressure drop increased ~10% and after the first cleaning, returned to the baseline condition for several days. However, after the next 30 days, pressure drop was 40% higher than baseline conditions, but

cleaning only lowered the pressure drop so that it was 20% above baseline. The third cleaning only reduced pressure drop from 100% higher than baseline to 60% higher than baseline. Visual inspection does not indicate substantial clogging of the warm seawater inlet (Figure 51). It is most likely that fouling/growth is on the plate surfaces and that growth is not removed by spraying the inlet with water.

U-value is predominantly determined by the external (warm seawater) flow rate. The baseline U-value test included testing different cold seawater flow rates for each warm seawater flow rate. The variation in U-value due to extremes in cold seawater flow rate is ~10%. For the same warm seawater flow rate, U-value has decreased by ~25% (Figure 50). This difference is not explained by variations in cold seawater flow rate. Rather, the decrease in U-value is further evidence that the surfaces of the plates are fouled. A film increases thermal resistance which lowers U-values and increases the surface roughness which increases pressure drop. It is unlikely that the film is thick enough to substantially change the effective channel size (for an observable increase in pressure drop).

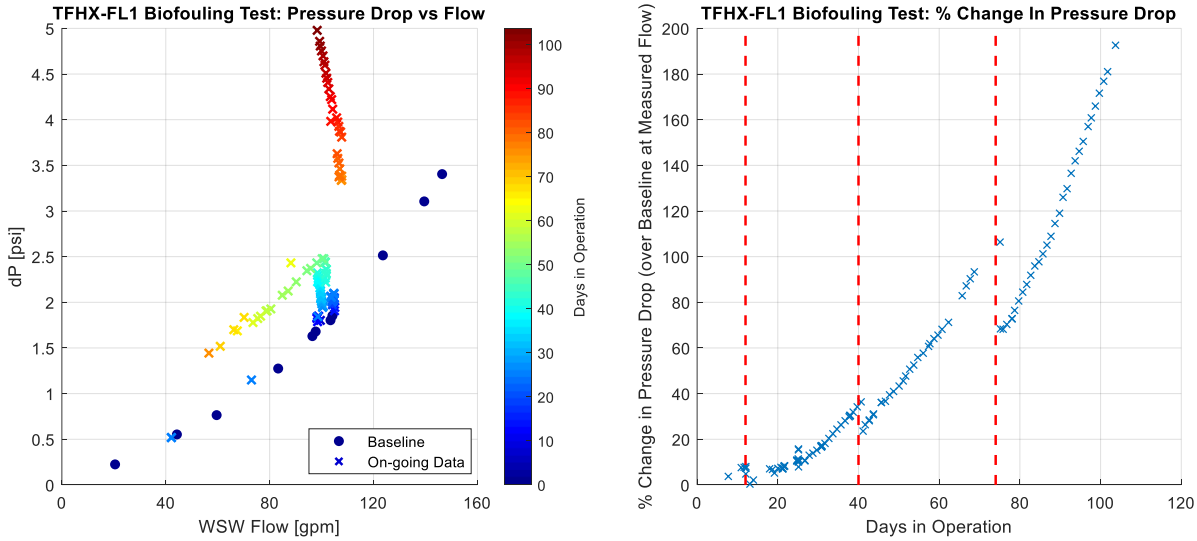

Figure 49. TFHX-FL1 biofouling test change in pressure drop over time.

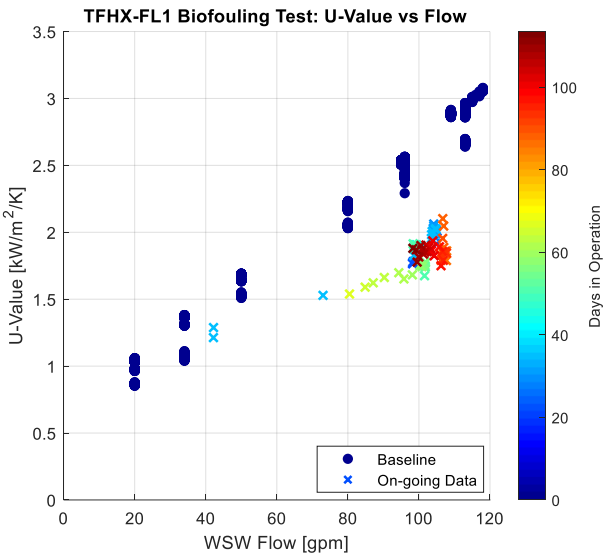

Figure 50. TFHX-FL1 biofouling test change in U-value over time.

Based on the results to date, monthly cleanings with water are insufficient to maintain the performance of a TFHX unit. Makai plans to disassemble the unit after 6 months to inspect the plate surfaces to confirm biofilm growth on the plate surfaces explains the decrease in performance. In parallel, Makai will come up with treatment methods for the next biofouling test unit as well as explore TFHX designs that are more easily cleaned.

1 month

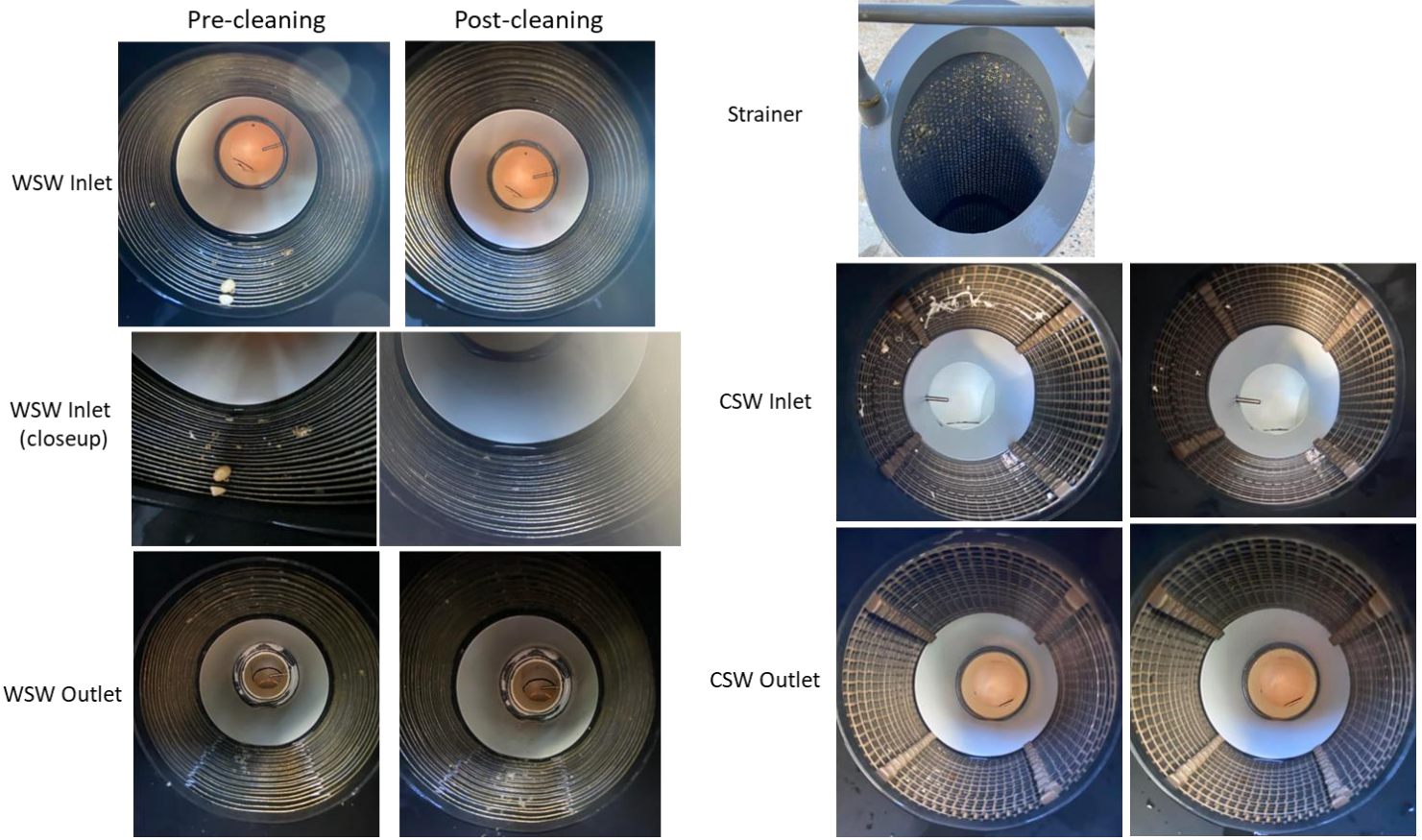
Pre-cleaning
Post-cleaning
WSW Inlet
WSW Inlet (closeup)
WSW Outlet
Pre-cleaning
Post-cleaning
Strainer
CSW Inlet
CSW Outlet

2 month

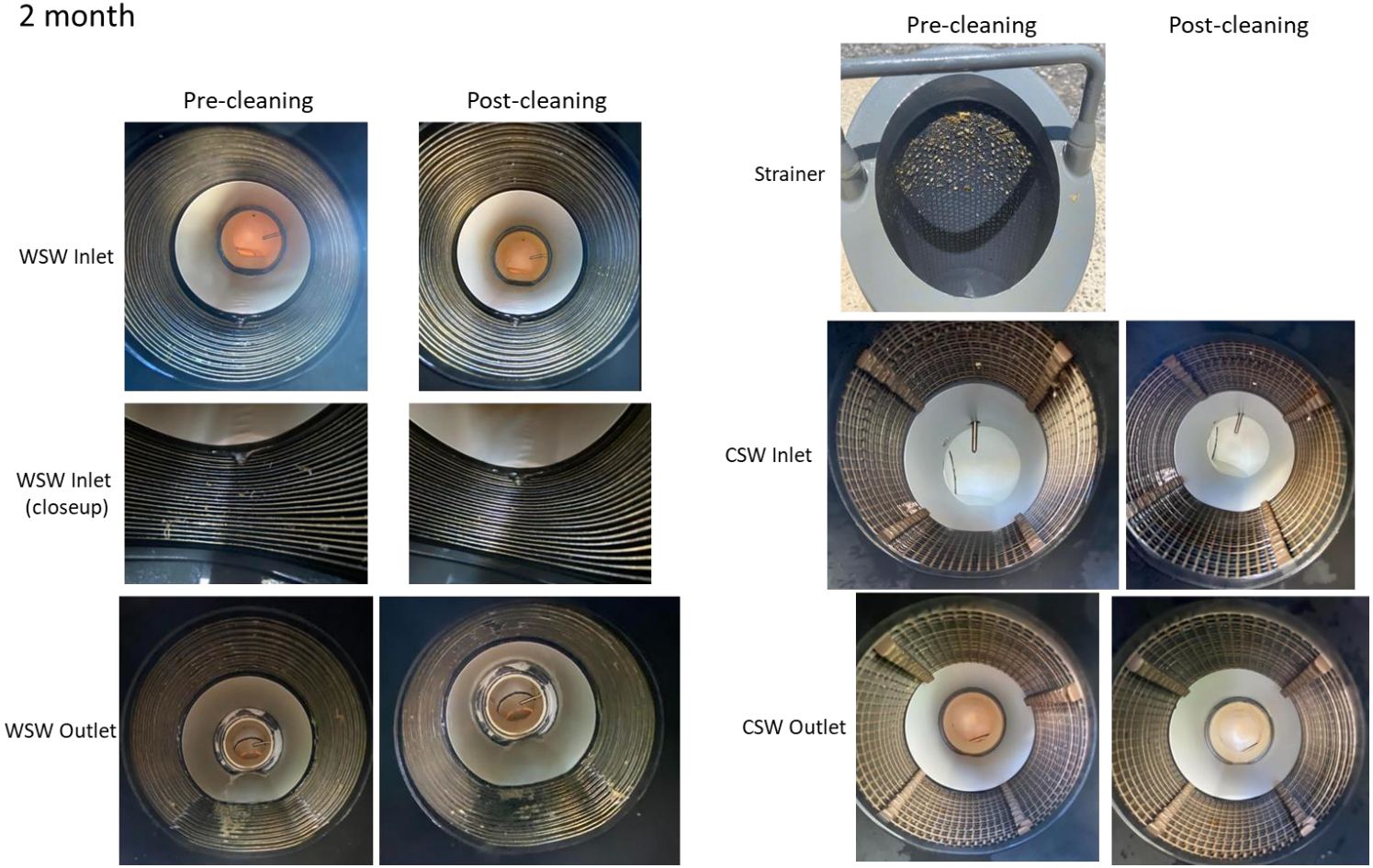
Pre-cleaning
Post-cleaning
WSW Inlet
WSW Inlet (closeup)
WSW Outlet
Pre-cleaning
Post-cleaning
Strainer
CSW Inlet
CSW Outlet

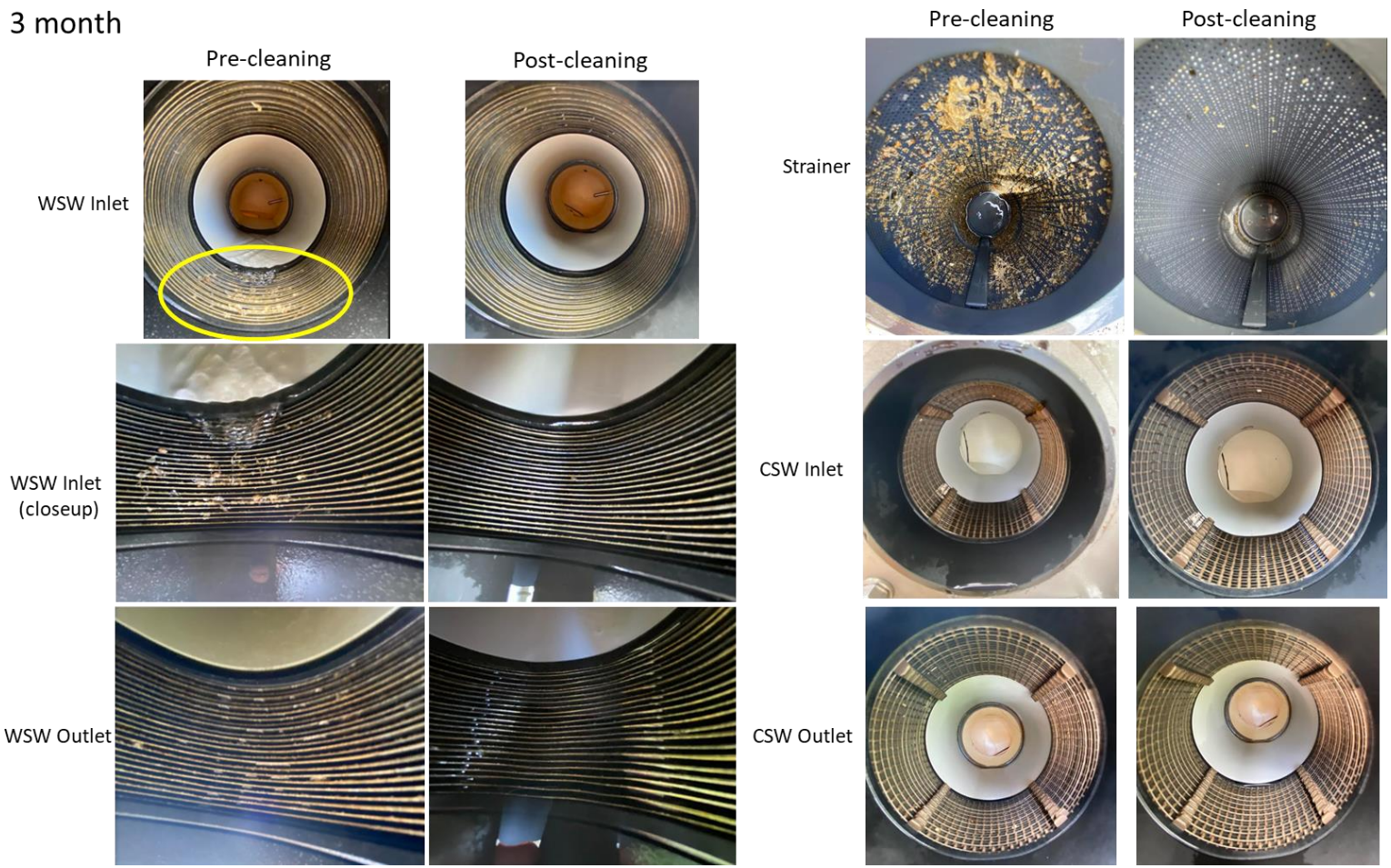

Figure 51. Pre- and post-cleaning images after 1, 2, and 3 months of testing.

6. ECONOMIC ANALYSIS

With over 10,000 welds on a single full-length plate, the importance of attaining a 99.9999% (1 defect in 1 million welds) vice 99.99% (1 defect in 10,000 welds) success rate is paramount to a cost competitive, economic TFHX. The current success rate at 1 defect in 10,000 welds translates to an overall 50% success rate for full-length plate fabrication. In this period, Makai reported difficulties in achieving high success rates while fabricating the full-length plates and incorporated success rate into the economic model to provide more realistic cost projections. Makai is exploring real-time imaging and other techniques (e.g., x-ray scanning) to identify and repair defective welds, but the effectiveness and time required for the repair process is currently unknown; once established, both repair time and repair success rate will be added to the economic model.

No substantial changes to the fabrication process were made in this period. The full-length plates used in FL1 – FL3 were constructed on the HSWS and each plate required, on average, 12 minutes to install, weld, and form. In the cutting station, it takes 2.5 minutes to install, cut, and remove the finished plate. Makai also added an additional 2.5 minutes per plate for a pressure check.

Compared to previously projected 4-port costs, current cost projections are slightly higher to reflect the plate success rate and added overhead costs. In the updated cost projection, improving the plate success rate from 50% to 90% reduces TFHX cost by 40% because the costs associated with plate success rate comprise 80% of the cost. However, with expected improvements to the plate success rate, continued improvement in fabrication methods, Makai expects a realistic cost for a 4-port, titanium, TFHX to approach $\$400/m^2$.

Finally, Makai previously reported on a pass-through design, which eliminates the module housing used in the 4-port design. Makai has been developing a low-cost design for an encapsulated pass-thru design. Makai believes this new design will capture performance benefits associated with a lower external pressure drop, maintenance benefits with cleaning access, and economic benefits of elimination module costs for a lower cost option.

7. CONCLUSION

Between August 2021-July 2022, Makai made significant progress in advancing the TFHX design, reducing TFHX fabrication time/cost, and adding empirical data to TFHX thermal, hydraulic, and structural/mechanical performance database. In doing so, Makai continues to gain expertise in the fundamental principles of laser welding and further our understanding of the TFHX technology.

TFHX Design and Characterization. Makai developed a welding analysis tool to guide weld parameter selection based on material and foil properties. Makai demonstrated the TFHX fabrication process could be used with Haynes 230 and stainless steel. The expanded material selection enabled higher pressure ratings, higher operating temperatures, and different channel sizes. Makai tested a new design targeted for higher pressure and higher temperature applications. The initial test identified design and procurement modifications for the next round of testing. Finally, Makai began another set of testing to identify processes to extend TFHX durability under cyclic pressure testing. Preliminary results indicate a 3X increase in cycles prior to failure can be achieved by implementing an additional process step.

TFHX Fabrication. Makai's on-going priority is to improve fabrication success rate by careful control of the welding environment and improving fixturing. A High Speed Pressure Tester (HSPT) was also commissioned to streamline quality control of leak checks. In the HSPT, a leak check can be started in less than 1 minute, which is significantly faster than previous fixtures.

Another way to improve the fabrication success rate is to repair weld defects. Makai has had some success repairing weld defects after a plate has completed all the fabrication steps. An alternative is to repair weld defects immediately after welding, which currently requires defects to be identified visual inspection. A manual process to inspect 10,000 welds per plate is not economical; therefore, Makai has started to develop automated real-time weld quality control methods using imaging and other monitoring tools to identify and repair weld defects after the welding step.

All-Welded Design. Makai was able to individually demonstrate the welds required to complete a sealed stack of all-welded plates, but limitations made it difficult to inspect the welds in place. A sealed stack was attempted but Makai was not able to demonstrate sealing. All-welded development was paused to focus on the fabrication success rate in the HSWS.

Stand-Alone TFHX Demonstration. In this period, Makai tested three ammonia-seawater (OTEC) TFHXs and three seawater-seawater (SWAC) TFHXs. Between the three FL units tested, larger ammonia-side channels and larger seawater channels were favored in condenser mode, whereas smaller ammonia channels and larger seawater channels were favored in evaporator mode. When evaluating the best design for an OTEC system, for a fixed seawater flow rates, for a fixed heat exchanger area, FL1 and FL2 produced the highest net power/m^3.

TFHX-FL2 was better suited for SWAC applications, but the internal pressure drop was too high for the HECO auxiliary cooling application. With a shorter plate and higher cooling water flow rate, a TFHX could match duty for comparable area and reduced heat exchanger pumping power but it is unclear if changes are possible.

Makai has learned that existing heating/cooling systems operate at conditions that accommodate the limitations of existing heat exchangers and those conditions are typically not favorable for a drop-in replacement TFHX. However, if operating conditions (i.e., flow rates, outlet temperatures) can be changed, TFHX designs can provide the required duty with overall savings in parasitic power.

Upcoming Work

The major points of focus for Makai's near-term work are to:

- Resolve fabrication success rate issues on the HSWS. Makai has moved the HSWS to a new fabrication facility and is developing weld quality monitoring tools.
- Develop an encapsulated, pass-through heat exchanger design that can be easily cleaned
- Fabricate additional full-length modules for performance and biofouling testing in ammonia-seawater and seawater-seawater orientations.
- Continue with geometric and mechanical characterization, with a focus on predicting TFHX durability.

8. APPENDIX A – TFHX PERFORMANCE TESTING

8.1. DATA ACQUISITION AND INSTRUMENTATION

A custom developed Labview-based program was used to collect data. The instruments (Table 5) output a 4-20 mA signal, proportional to the measurement, which was read using National Instruments' NI 9208 Analog Input modules. Measurements were sampled 10X a second, averaged, and recorded every second.

Table 5. Sensors Used in TFHX Performance Testing

Measurement	Model	Range	Accuracy
Seawater Flow Rate	Rosemount 8705 Mag Meter	0-300 gpm	0.25% of rate
Ammonia Vapor Flow Rate	Micromotion Coriolis CMFS075M	0.03-1.74 kg/s	0.25% of rate
Ammonia Liquid Flow Rate	Micromotion Coriolis CMFS075M	0.03-1.74 kg/s	0.25% of rate
Seawater Inlet/Outlet Temperatures (Seawater-Ammonia Testing)	IsoTeach milliK	0-100 C	0.01 C
Seawater Inlet/Outlet Temperatures (Seawater-Seawater Testing)	Intempco MIST 55	0-50 C	0.1 C + 0.1% FS
Seawater Inlet/Outlet Pressure	GE UNIK5000	0-30 psia	0.25% FS*
Ammonia Inlet/Outlet Temperature	Intempco MIST 55	0-50 C	0.1 C + 0.1% FS
Ammonia Inlet/Outlet Pressure	GE UNIK5000	400-1100 kPa gauge	0.25% FS*

* Another +/- 0.5% FS due to temperature error band needs to be added to the stated static accuracy. In practice, the pressure sensors are accurate to +/- 1 kPa.

8.2. TEST MATRIX

Test points for condenser, evaporator, and seawater-seawater testing for each unit are summarized in Table 6 through Table 14.

8.2.1. TFHX-FL-1 Test Points

Table 6. TFHX-FL-1 Condenser Test Points

		Energy Density [kW/m2]						
		4.84	7.27	8.24	9.69	10.66	11.63	12.60
Seawater Velocity [m/s]	0.30	X	X	X	X			
	0.40	X	X	X	X	X	X	X
	0.43	X	X	X	X	X	X	
	0.53	X	X	X	X	X	X	
	0.67	X	X	X	X	X	X	
	0.80	X	X	X	X	X	X	
	0.88	X	X	X	X	X	X	
	1.04	X	X	X	X	X	X	
	1.18	X	X	X	X	X	X	X
	1.33	X	X	X	X	X	X	X

Table 7. TFHX-FL-1 Evaporator Test Points

		Energy Density [kW/m2]					
		4.74	5.92	7.10	8.29	9.47	10.06
Seawater Velocity [m/s]	0.46	X	X	X	X	X	
	0.72	X	X	X	X	X	X
	0.83	X	X	X	X	X	X
	0.91	X	X	X	X	X	X
	1.02	X	X	X	X	X	X
	1.09	X	X	X	X	X	X
	1.15	X	X	X	X	X	X
	1.23				X	X	X
	1.32				X	X	X

Table 8. TFHX-FL-1 Seawater-Seawater Test Points

		Internal Seawater Velocity [m/s]									
		0.10	0.16	0.20	0.22	0.27	0.32	0.36	0.42	0.47	0.53
External Seawater Velocity [m/s]	0.05	X				X		X			
	0.06	X	X		X					X	
	0.06						X		X		
	0.11		X		X	X	X	X	X	X	
	0.14						X				
	0.20		X	X		X		X	X	X	
	0.33		X	X	X	X	X	X	X	X	X
	0.39		X	X		X		X	X	X	
	0.47					X	X	X	X	X	X
	0.53					X		X	X	X	
	0.57					X					
	0.62						X		X	X	
	0.66										
	0.74						X	X	X	X	X
	0.94								X	X	X
	1.13									X	X

8.2.2. TFHX-FL-2 Test Points

Table 9. TFHX-FL-2 Condenser Test Points

		Energy Density [kW/m2]				
		2.5	5	7.5	10	12.5
Seawater Velocity [m/s]	0.17	X				
	0.29	X	X	X		
	0.38	X	X		X	
	0.46	X	X	X	X	X
	0.53	X	X	X	X	
	0.59	X	X	X	X	
	0.71	X			X	X
	0.81	X	X	X	X	X
	0.89	X				X

Table 10. TFHX-FL-2 Evaporator Test Points

		Energy Density [kW/m2]				
		2.5	5	7.5	10	12.5
Seawater Velocity [m/s]	0.18	X	X			
	0.30	X	X	X		
	0.40	X	X	X	X	
	0.46	X		X	X	
	0.53	X	X	X	X	
	0.59	X	X	X	X	
	0.71	X	X	X	X	
	0.79	X	X	X	X	X
	0.88	X	X	X	X	X

Table 11. TFHX-FL-2 Seawater-Seawater Test Points

		Internal Seawater Velocity [m/s]								
		0.07	0.12	0.15	0.24	0.29	0.35	0.40	0.44	0.52
External Seawater Velocity [m/s]	0.10	X	X	X	X	X	X	X		
	0.18		X	X		X				
	0.19			X	X		X	X	X	X
	0.31			X	X	X	X	X	X	X
	0.40				X	X	X	X	X	X
	0.48				X	X	X	X	X	X
	0.54				X	X	X	X	X	X
	0.60					X	X	X	X	X
	0.67					X	X	X	X	X
	0.72					X	X	X	X	X
	0.82						X	X	X	X
	0.91							X	X	X
	1.00								X	X

8.2.3. TFHX-FL-3 Test Points

Table 12. TFHX-FL-3 Condenser Test Points

		Energy Density [kW/m2]						
		5	7.5	10	12.5	15	17.5	20
Seawater Velocity [m/s]	0.43	X	X	X	X	X	X	X
	0.57	X	X	X	X	X	X	X
	0.66	X	X		X	X	X	X
	0.75	X	X	X	X	X	X	X
	0.84	X	X	X	X	X	X	X
	0.91	X		X		X	X	X
	0.94			X			X	
	1.03	X	X	X	X	X	X	

Table 13. TFHX-FL-3 Evaporator Test Points

		Energy Density [kW/m2]				
		7.5	10	12.5	15	17.5
Seawater Velocity [m/s]	0.42		X	X	X	X
	0.55	X	X	X	X	X
	0.61	X	X	X	X	X
	0.70	X	X	X	X	X
	0.77	X	X	X	X	X
	0.84	X	X	X	X	X
	0.98	X	X	X	X	X
	1.05	X	X	X	X	

Table 14. TFHX-FL-3 Seawater-Seawater Test Points

		Internal Seawater Velocity [m/s]												
		0.23	0.29	0.35	0.40	0.45	0.48	0.52	0.59	0.61	0.62	0.70	0.75	0.79
External Seawater Velocity [m/s]	0.26	X	X	X	X	X	X	X	X	X	X	X	X	X
	0.31	X	X	X	X	X	X	X	X		X	X	X	X
	0.34	X	X	X	X	X	X	X	X		X	X	X	X
	0.38	X	X	X	X	X	X	X	X		X	X	X	X
	0.49		X	X	X	X	X	X	X		X	X	X	X
	0.56			X	X	X	X	X	X		X	X	X	X
	0.60			X	X	X		X	X	X	X	X	X	X
	0.64				X	X	X	X	X	X	X	X	X	X
	0.69				X	X	X	X		X	X	X	X	X
	0.75				X	X	X	X		X	X	X	X	X
	0.82					X	X	X		X	X	X	X	X
	0.93						X	X		X	X	X	X	X
	1.01								X	X			X	X
	1.07								X	X	X	X	X	
	1.15								X		X	X	X	X
	1.25										X	X	X	X
	1.39													X
	1.51												X	X
	1.61													X

8.3. CALCULATED VALUES

Several values are calculated by the 100 kW control software in real time. These values are used in determining steady state operation and characterizing heat exchanger performance.

8.3.1. Fluid Properties

Seawater properties used in mass flow rate and duty calculations are summarized in Table 15.

Table 15. Seawater properties used in seawater calculations

	Condenser	Evaporator
Temperature	6 °C	26.5 °C
Salinity	34.7 ppt	34.7 ppt
Density	1027.3 kg/m^3	1022.8 kg/m^3
Kinematic Viscosity	1.53E-6 m^2/s	9.26E-07 m^2/s
Thermal Conductivity	0.580 W/m/K	0.609 W/m/K
Prandtl Number	10.815	6.224

Ammonia fluid properties are calculated at the measured temperature and pressure using REFPROP10.

8.3.2. Seawater Mass Flow Rate

Seawater mass flow rate is calculated from the measured volumetric flow rate:

$$\dot{m} = \frac{gpm}{15850.3\ {}^{gpm}/_{m^3/s}} \times \rho$$

The density of cold seawater is taken to be 1027.3 kg/m^3 and the density of warm seawater is taken to be 1022.8 kg/m^3.

8.3.3. LMTD

LMTD is a measure of the average temperature difference across the heat exchanger. It is used in the calculation of overall heat transfer coefficient, U. LMTD is calculated according to:

$$LMTD = \frac{(T_{wsw\ in} - T_{csw\ out}) - (T_{wsw\ out} - T_{csw\ in})}{\ln \frac{T_{wsw\ in} - T_{csw\ out}}{T_{wsw\ out} - T_{csw\ in}}}$$

8.3.4. Duty

Duty is a measure of the heat transferred between warm and cold seawater and is used in the calculation of overall heat transfer coefficient. Duty can be calculated based on eitherseawater or based on the ammonia. The equations used to calculate the duty are:

$$Duty_{wsw} = \dot{m_{wsw}} * c_{p,wsw} * (T_{wsw\ in} - T_{wsw\ out})$$

$$Duty_{csw} = \dot{m_{csw}} * c_{p,csw} * (T_{csw\ out} - T_{csw\ in})$$

$\dot{m}$ = mass flow rate [kg/s],

c_p = specific heat capacity of seawater [kJ/kg],

T = seawater temperature [C], and

8.3.5. Overall Heat Transfer Coefficient

The overall heat transfer coefficient, U, is a measure of the overall efficiency of a heat exchanger. It is calculated according to:

$$U = \frac{Duty}{LMTD * Area}$$

LMTD = log mean temperature difference [C]

Area = heat transfer area of the heat exchanger [m^2]

Both duty and LMTD directly impact the calculation of overall heat transfer coefficient. The duty used to calculate the heat transfer coefficient is the ammonia duty.

8.3.6. Convective Heat Transfer Coefficients

The overall heat transfer coefficient is a function of the convective and conductive heat transfer coefficients:

$$\frac{\mathbf{1}}{\boldsymbol{UA}} = \frac{\mathbf{1}}{\boldsymbol{h_{csw}A}} + \frac{\boldsymbol{t}}{\boldsymbol{k_{foil}A}} + \frac{\mathbf{1}}{\boldsymbol{h_{wsw}A}} \qquad \textit{Equation 8-1}$$

where

A = heat transfer area [m^2],

h_{csw} = internal seawater convective coefficient [kW/m^2C],

h_{wsw} = external seawater convective coefficient [kW/m^2C],

t = foil thickness [m], and

k_{foil} = thermal conductivity of titanium foil [kW/mC],

The heat transfer area for each component in Equation 3-1 is the same; Equation 3-1 reduces to:

$$\frac{\mathbf{1}}{\boldsymbol{U}} = \frac{\mathbf{1}}{\boldsymbol{h_{SW}}} + \frac{\boldsymbol{t}}{\boldsymbol{k_{foil}}} + \frac{\mathbf{1}}{\boldsymbol{h_{NH3}}} \qquad \textit{Equation 8-2}$$

1/U is calculated from the data as described in Section 8.3.5. t/k_{foil} is a constant based on the physical and thermodynamic properties of the foil.

In order to determine h_{csw} and h_{wsw}, the internal and external seawater-side heat transfer coefficient was assumed to be constant for a fixed seawater flow rate and independent from the other side. By holding internal seawater flow rate constant and changing the external seawater flow rate and vice versa, a matrix of U-values for each combination of internal/external seawater flow rates was generated. The entire set of equations was solved simultaneously using the method of constrained least squares.

8.4. DATA PROCESSING

Raw data were first graphed in a custom analysis program. Large sections of data could be quickly reviewed and steady-state data was averaged and added to a summary file. Sections of steady-state data were added to a separate file.

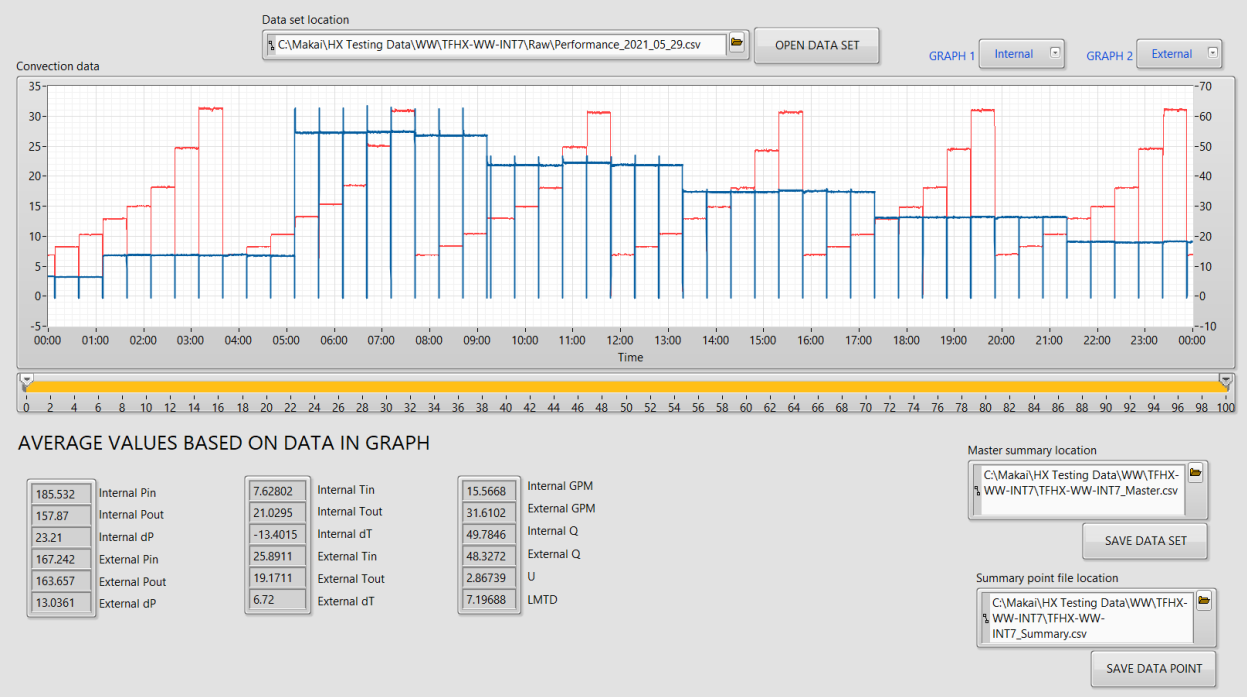

Figure 52. Data review program is first used to identify sections of steady-state data. For each section, an averaged set of values is saved in a summary file and all points in the section are saved in a master data file.

Summarized data points were grouped by internal/external flow rates, with a range of +/- 3% of gpm for most flows but up to +/-10% for the lowest flow rates. The lower flow rates were highly sensitive to fluctuations in system pressure and difficult to consistently return to the same flow rate.